Solar Physics
DOI: 10.1007/●●●●●-●●●-●●●-●●●●-●

Reconciliation of Observational Challenges to the Impulsive-Piston Shock-Excitation Scenario. I. Kinematic Challenges

V.V. Grechnev · V.I. Kiselev · A.M. Uralov

Received ; accepted

Abstract Until now, there is no consensus on the origin of coronal shock waves. Questions also remain about the patterns that govern the propagation of the presumably related disturbances observed in the extreme ultraviolet (EUV waves). We present arguments in favor of the initial excitation of the waves by the impulsive acceleration of erupting structures. We consider two puzzling events that have been known thanks to the efforts of different research teams. Using recent findings and our methods, we aim to figure out what might actually have happened in these challenging events. In the first event, the expansion of the coronal mass ejection (CME) was determined by gravity starting from the low corona. The previous analysis led the authors to a conclusion about the flare-related origin of the associated shock wave. We also consider another event, in which an EUV wave had a strange kinematics. This was one of the weakest flares accompanied by EUV waves. Both of these challenging events have been reconciled in terms of an impulsively-excited piston shock.

Keywords: Coronal Mass Ejections; Flares; Radio Bursts, Type II; Waves, Shock

✉ V.I. Kiselev
valentin_kiselev@iszf.irk.ru

V.V. Grechnev
grechnev@iszf.irk.ru

A.M. Uralov
uralov@iszf.irk.ru

Institute of Solar-Terrestrial Physics SB RAS, Lermontov St. 126A, Irkutsk 664033, Russia

1. Introduction

The existence of shock waves propagating in the solar corona and interplanetary space is generally accepted. Shock waves in the lower corona are manifested in metric Type-II radio bursts and near-surface disturbances that travel more or less rapidly over large distances (comparable to the solar radius) and can be observed in different spectral ranges such as the Hα line (Moreton waves: Moreton, 1960; Uchida, 1968, 1974; Warmuth et al., 2004a,b; Balasubramaniam, Pevtsov, and Neidig, 2007), the extreme ultraviolet (EUV waves or EIT waves: Moses et al., 1997; Thompson et al., 1998, 1999; Warmuth et al., 2001; Warmuth, 2010), and others (Vršnak et al., 2002; Hudson et al., 2003; White and Thompson, 2005; Warmuth, Mann, and Aurass, 2005; Warmuth, 2007, 2015). At longer distances, shock waves are manifested in Type-II emissions of the decametric to hectometric ranges (Cane and Erickson, 2005; Bougeret et al., 2008), while their traces appear in coronagraph white-light images as faint halos surrounding fast coronal mass ejections (CMEs) and deflections and kinks of coronal rays (e.g. Uralova and Uralov, 1994; Vourlidas et al., 2003; Gopalswamy et al., 2009; Feng et al., 2012, 2013; Shen et al., 2013). Shock waves propagating farther in the interplanetary space are manifested in the kilometric Type-II emission and are detected in situ from discontinuities in plasma parameters and magnetic field by sensors of space missions at different locations in the heliosphere even well beyond the Earth's orbit (e.g. Luhmann et al., 2008; Liu et al., 2008; Echer, 2019).

Shock waves generated in solar storms can be associated with space-weather disturbances. Shocks driven by fast interplanetary CMEs (ICMEs) mark sudden commencements of geomagnetic disturbances, though they alone are unlikely to produce intense geomagnetic storms (Echer et al., 2008). The role of shock waves in the acceleration of protons and heavier ions, at least to low and moderate energies, is widely accepted (Klein and Trottet, 2001; Dierckxsens et al., 2015; Trottet et al., 2015). Moreover, a number of researchers consider the shocks as the only accelerator of heavy particles that appear in the interplanetary space (e.g. Kahler, 2001; Reames, 2013; Gopalswamy et al., 2014; Cliver, 2016). Near-Earth proton enhancements pose hazard to equipment and astronauts on spacecraft and to crew members and passengers of transcontinental flights that enter high latitudes, due to secondary particles produced in interactions of solar protons with the Earth's atmosphere (e.g. Veselovsky et al., 2004). To find out under what conditions shock waves accelerate particles, it is important to know their development and evolution (see, e.g., Reames, 2009; Gopalswamy et al., 2012).

Although the shock-wave excitation mechanisms have been known for several decades, observational limitations make it difficult to reliably determine which of them is responsible for the appearance of a coronal shock in a particular event (see, e.g., the review by Vršnak and Cliver, 2008). This has made the origin of shock waves controversial. Based on the supposed analogy between a solar flare and a thermal explosion, the first concept related shock-wave excitation to flares (Moreton, 1960; Uchida, 1968, 1974). Next, Hirayama (1974) have proposed that a shock wave is generated by a rising prominence, whose eruption is caused by a current instability. Further, in situ measurements of shocks ahead of fast ICMEs favored the initial bow-shock excitation by the outer surface of a CME

when its speed becomes super-Alfvénic (e.g. Cliver et al., 2004; Reames, 2009; Gopalswamy et al., 2009, 2013; Rouillard et al., 2016). Cane (1984) and Cane and Erickson (2005) have raised concern about a possible distinction between coronal and interplanetary shock waves. Conversely, Kalaivani et al. (2021) have concluded that Type-II emissions often continue from meters to kilometers.

The character of the shock-wave excitation and their subsequent evolution contain essential information about solar sporadic phenomena. Clarification of responsibility for the shock-wave appearance of an impulsive or quasi-stationary process and its specific driver can shed light on different classes of flares and eruptions, the CME formation processes, and relationships between CMEs and their progenitors. These aspects of studies of shock waves complement their space-weather impact and other applications outlined by Warmuth (2007, 2015).

Some studies propose different shock-excitation scenarios (e.g. Nindos et al., 2011; Eselevich, Eselevich, and Zimovets, 2013; Eselevich et al., 2015; Su et al., 2015; Rouillard et al., 2016). The presence of a shock and a fast CME is often postulated as the initial bow-shock appearance. Flare generation of blast waves is also advocated (Magdalenić et al., 2008, 2010, 2012; Kumar and Innes, 2013, 2015; Kumar, Innes, and Cho, 2016; Eselevich, Eselevich, and Zimovets, 2019).

Case studies of several eruptive flares have led Grechnev et al. (2011a, 2013, 2016, 2018a,b) to a conclusion that shock waves initially appear as piston shocks impulsively excited by erupting filaments, as Hirayama (1974) proposed. Bain et al. (2012) and Zimovets et al. (2012) made similar conclusions. Then, the piston shock transforms either into a bow shock, if the CME is fast, or into a blast wave, if the CME is slow or absent (Zimovets et al., 2012; Grechnev et al., 2015, 2017). In the blast-wave regime without the energy supply from a piston, the shock wave decays soon and becomes a weak magnetosonic disturbance.

Invoking theoretical considerations, these studies have shown that the shock-excitation by the flare pressure pulse meets difficulties, while the bow-shock excitation is possible only in the regime of the supersonic plasma flow around the wave driver. An example is the uniform motion at a supersonic speed of a constant-shape body in a homogeneous gas. Here the velocities of the bow shock and the body are equal and the mass of gas between them does not change. However, during the early eruption, the extrusion of plasma surrounding the expanding structure dominates over the plasma flow around it. The wave driver is a quasi-spherical magnetic piston. The plasma mass between its surface and the wave front rapidly increases. The piston accelerates impulsively, while the relation between its maximum speed and the fast-mode speed [$V_{\rm fast}$] does not affect the character of the appearing piston shock. For these reasons, the piston shock appears earlier than the bow shock. The plasma speed behind the piston shock is subsonic and not supersonic (Landau and Lifshitz, 1987), as required for the bow-shock appearance. This makes it impossible for the bow shock to form soon behind the piston shock. The situation can change after some time, when the plasma flow around the piston becomes significant and the distance between the decelerating piston shock and piston decreases. The piston shock gradually transforms into a bow shock, if the piston is fast enough.

Uralov, Grechnev, and Ivanukin (2019) developed a common theoretical description of the impulsive piston-shock excitation, its propagation inside an

emerging CME, and further ahead of it. The conflict between this concept and the conclusions of the studies mentioned raises the question of whether different shock-excitation mechanisms are implemented or the observations addressed in these studies can be reconciled in terms of an impulsively-excited piston shock.

The possibility of transforming a piston shock into a bow shock can hide its prime cause. It is also hidden for a shock wave that, being initially an impulsively-excited piston shock, "detaches" from the piston, which has switched to deceleration, and propagates away, resembling a blast wave. The kinematics of such waves of ample intensity can be described by the relations of the point-explosion theory or by the methods of nonlinear acoustics, if the wave intensity is low (Afanasyev and Uralov, 2011; Afanasyev, Uralov, and Grechnev, 2013).

The shock-wave regime can be identified from in-situ measurements from the plasma density distribution behind the shock, but it is more difficult to recognize it from remote observations. For this purpose, kinematic measurements, comparison and relative timing of the observed shock-wave signatures with each other and with expectations for a piston shock, and other indications are used.

Wave-like coronal disturbances, including shock waves, also appear as EUV waves. Efforts by a number of researchers have shown that EUV waves are due to different phenomena (Biesecker et al., 2002; Zhukov and Auchère, 2004; Warmuth, 2007, 2010, 2015; Warmuth and Mann, 2011; Chen, 2011; Gallagher and Long, 2011; Patsourakos and Vourlidas, 2012). These are: i) magnetosonic waves (and shock waves), ii) compressed plasma layers on top of erupting structures, and iii) field-line-stretching effect (Chen et al., 2002; Chen, Fang, and Shibata, 2005). Different phenomena can coexist in one event (Chen and Wu, 2011; Grechnev et al., 2011b). EUV waves provide information about the disturbances produced in solar events, but the difference in the processes causing them with the similarity of manifestations complicates their interpretation.

Observational capabilities have greatly improved in the last 15 years. The twin *Solar-Terrestrial Relations Observatory* (STEREO: Kaiser et al., 2008) with the *Sun Earth Connection Coronal and Heliospheric Investigation* instrument suite (SECCHI: Howard et al., 2008) in 2006 started observing the Sun from different vantage points with an enhanced imaging rate. The *Atmospheric Imaging Assembly* (AIA: Lemen et al., 2012) on board the *Solar Dynamics Observatory* (SDO: Pesnell, Thompson, and Chamberlin, 2012) since 2010 observes the Sun with a high spatial and temporal resolution. The advanced observations and modeling (e.g. Žic et al., 2008; Lulić et al., 2013; Liu and Ofman, 2014; and listed above) provide new insight on EUV waves and the shock-wave evolution. However, there is still no complete clarity and consensus on these issues. The questions raised by studies of challenging events remain unanswered.

Our two companion articles address a few challenging events, all of which were studied previously, and reconcile their observations in terms of an impulsively-excited piston shock. We find out what actually occurred in these events and reveal their interesting aspects that were not detected so far. The present article (hereafter Article I) addresses two events with strange kinematics. Article II (Grechnev et al., 2022) addresses four CME-less events that were presented as candidates for different shock-excitation scenarios.

Section 2 discusses the shock-excitation scenarios and presents analytic descriptions of the propagation of an impulsively-excited piston shock and the

trajectories of Type-II bursts. Section 3 analyzes the event, in which strange kinematics reconstructed for the CME led the authors to the conclusion that a shock wave was excited by a flare. Section 4 addresses another event, in which odd kinematics of an EUV wave led the authors to the idea of a complex rise of an erupting filament. We reveal two magnetosonic EUV waves in this event. Section 5 summarizes the results and outlines their implications.

2. Basic Considerations and Methodical Issues

2.1. Typical Shock-Wave Histories

Its is widely accepted that a typical driver of an eruption is a flux rope, whose main poloidal flux is formed due to magnetic reconnection that also produces a flare (Inhester, Birn, and Hesse, 1992; Qiu et al., 2007; Longcope and Beveridge, 2007; Vršnak, 2016). A probable flux-rope progenitor is a filament (prominence), whose magnetohydrodynamic (MHD) instability leads to the eruption (Hirayama, 1974; Uralov et al., 2002; Grechnev et al., 2006a). The rising filament forces overlying magnetic structures to expand, including the separatrix surface between them and the streamer above. The expanding separatrix surface piles up plasma that makes up an increasing compressed layer above the flux-rope progenitor, which transforms into a flux rope.

A sharp expansion of the erupting filament causes a strong MHD disturbance formed as a simple wave. Propagating omnidirectionally, it enters the regions, where the fast-mode speed steeply decreases from its high value above an active region. The leading wave packets slow down, while the next ones arrive. The disturbance undergoes jamming, its profile is steepened, and the shock discontinuity is rapidly formed. Afanasyev, Uralov, and Grechnev (2013) estimated the shock formation time to be 10^2 seconds for an acceleration of the driver (erupting filament) of $1\,\mathrm{km\,s^{-2}}$ that can be shorter for a stronger acceleration. A piston shock (Vršnak and Cliver, 2008) is impulsively excited inside a developing CME, propagates outward, and appears ahead of expanding structures. The initial speed of the piston shock is high, being determined by the fast-mode speed above the parent active region, and exceeds the speed of the driver. This chain of events was observed by Grechnev et al. (2016) and addressed theoretically by Uralov, Grechnev, and Ivanukin (2019).

As the latter study shows, such a shock gains energy from the piston expanding behind it that determines their self-similarity for some time. On the other hand, the piston gains energy due to the work of the forces responsible for the MHD instability during the eruption. Shortly after the acceleration stage, the piston only spends energy to overcome gravity and to extrude the plasma from the volume that it occupied previously. At this stage, the piston+piston-shock system does not gain additional energy. Due to the conservation of the energy integral in the volume where the movement occurs, the situation resembles a decelerating gas-dynamic blast wave produced by a point explosion (Grechnev et al., 2008). If the CME is fast, then eventually, when the plasma extrusion regime is replaced by the plasma flow around the CME, then the piston shock is

transformed into a bow shock. Otherwise, the piston shock decays into a weak disturbance, if the CME is slow or absent (e.g. Grechnev et al., 2015, 2018a).

One might expect that a bow shock initially appears ahead of a gradually accelerating CME initiated by the eruption of a quiescent prominence away from active regions. Nevertheless, Grechnev and Kuzmenko (2020) revealed the impulsive-piston scenario in such an event. We are aware of the only candidate event for the initial bow-shock excitation (Fainshtein and Egorov, 2019).

2.2. Quantitative Description of the Shock Propagation

The piston-shock evolution described in Section 2.1 clarifies a quantitative description of its kinematics presented by Grechnev et al. (2008). The formation of a compressed layer surrounding the erupting structures considerably changes the plasma density distribution near the eruption region before the onset of the piston shock relative to static conditions. The situation is well described by the power-law model of the density distribution (Grechnev et al., 2008, 2011a):

$$n(x) = n_0(x/h_0)^{-\delta} \tag{1}$$

where x is the distance from the wave source located not high above the solar surface, n_0 is the density at a distance $h_0 = 100\,\mathrm{Mm}$ that is close to the scale height, and the density falloff exponent $[\delta]$ is generally direction-dependent. The argument in standard density models is the heliocentric distance $[r]$ measured in solar radii. In the radial direction, with $n_0 = 4.1 \times 10^8$ cm^{-3}, $\delta = 2.6$, and $x \approx (r-1)\mathrm{R}_\odot$ being the height above the photosphere, the power-law model is close to the equatorial Saito model (Saito et al., 1970) at distances $x > 0.4\mathrm{R}_\odot$, differing from it within $\pm 30\,\%$. At lower altitudes, the power-law model provides higher densities, reflecting a compressed layer growing during the eruption.

The piston spends energy to pile up and extrude plasma, supporting the piston shock. After the acceleration phase the piston slows down that determines deceleration of the piston shock, as in the case of a freely propagating blast wave:

$$x(t) \propto (t - t_0)^{2/(5-\delta)}, \tag{2}$$

where t_0 is the wave onset time. This equation is convenient to use in the form

$$x(t) = x_1[(t - t_0)/(t_1 - t_0)]^{2/(5-\delta)}, \tag{3}$$

where x_1 is the distance between the wave source and its front at time t_1.

The wave onset time is temporally close to the peak of the acceleration pulse, which can precede a hard X-ray (HXR) or microwave burst by up to two minutes (e.g. Grechnev et al., 2013, 2015, 2016). Miklenic, Veronig, and Vršnak (2009) found a similar relation between the magnetic-flux change rate and HXR in some events. The density-falloff exponent $[\delta]$ determines the convexity of the distance–time plot, being typically between 2.5 and 2.9 for the radial motion away from the Sun and around 2.0 for EUV waves propagating along the solar surface.

2.3. Flare-Generated Blast Wave

Historically, the first hypothesis was the excitation of a blast wave by a pulse of thermal pressure of the flare plasma. The flare-related shock origin seems preferable if its exciter exhibits impulsive properties (e.g. the case of a Moreton wave: Moreton, 1960; Uchida, 1968, 1974), or if the estimated kinematic characteristics of the shock wave and CME differ significantly from each other, and especially if a CME is absent. However, the role of the flare pressure in the shock-wave excitation is unlikely (Grechnev et al., 2011a, 2015) for the following reasons:

i) Soft X-ray (SXR) images of hot flare structures show stable sources that do not expand dramatically to cause a strong disturbance that could become a shock wave. Motions of coronal loops observed in the extreme ultraviolet (EUV) are caused either by a CME or by a disturbance that appeared outside these loops or below them. However, EUV observations do not reveal sharp own motions of flare loops, in contrast to erupting structures.

ii) The plasma density and temperature in flare loops are manifested in their SXR emission that is recorded by the *Geostationary Operational Environmental Satellites* (GOES). The SXR emission is intrinsically gradual, being similar to the indefinite integral of the corresponding HXR burst (the Neupert effect: Neupert, 1968) that resembles the acceleration of an erupting structure (Temmer et al., 2008, 2010; Grechnev et al., 2013, 2015, 2016), which produces an MHD disturbance. Conversely, the plasma pressure in flare loops estimated from GOES SXR fluxes increases gradually.

iii) The plasma pressure in flare loops cannot considerably exceed the magnetic pressure, being compensated by the dynamic pressure of the reconnection outflow. The increase in the volume of flare loops is basically insufficient to produce a noticeable MHD outward disturbance. For example, if the plasma pressure in a flare loop becomes comparable with the magnetic pressure ($\beta \approx 1$) or even extremely high ($\beta \approx 10$), the effect is as small as an increase in each of its three dimensions by a factor of $(\beta + 1)^{1/4}$ (see Grechnev et al., 2006b for details). Moreover, an inherent property of emerging flare loops is not expansion, but contraction along with the reconnection outflow.

Let us nevertheless assume the possibility of a sharp plasma-pressure increase in flaring structures. We firstly discuss the possibility to generate short and weak shock waves directly by the flare current sheet. The impulsive phase of reconnection that leads to its tearing is accompanied not only by the acceleration of charged particles, generation of plasma flows and turbulence. At the place of the tearing, impulsive plasma heating and its explosive expansion also occur (Bogdanov et al., 1984). Since the energy of such an explosion is difficult to estimate, one can instead compare the characteristic size of the high-pressure zone with the size of fine structures in the current sheet, such as magnetic islands.

For an approximate solution to the linear problem on the decay of a volumetric pressure pulse, we define the region of an excessive pressure $[P]$ as a ball of radius

r_0. At a sufficient distance [r] from the current sheet, the pressure perturbation would be a blast N-wave of duration $2r_0/V_{\rm fast}$ and amplitude $(P/2)(r_0/r)$. Since r_0 is a characteristic size of a fine structure in the current sheet, i.e. a small value, so the length of the blast wave is very small and its amplitude dies out not far from its origin. Such "microscopic" shock waves are beyond our scope.

Flare structures not involved in the eruption are tied to magnetic topological elements in the flare region and change location quite smoothly. The generation of a wave disturbance by such structures should be considered in terms of the monopole mechanism (Uralov, Grechnev, and Ivanukin, 2019). The disturbance intensity is determined by the rate of change in the volume of a given structure.

We qualitatively use the solution to the linear problem of the sound-wave radiation by a pulsating sphere of radius r_0. The polars of the group and phase velocities of the fast magnetic sound in the corona above active regions (plasma $\beta \ll 1$) are equal circles, as for ordinary sound. The sound speed [$c_{\rm s}$] in Equation 4 adopted from Lependin (1978) can be replaced with $V_{\rm fast}$. When $(kr)^2 \gg 1$ approaching the wave zone, the amplitude u of the harmonic component of the plasma velocity in the disturbance caused by the pulsating sphere is

$$u = u_0 \left[kr_0 / \left(1 + (kr_0)^2\right)^{1/2} \right] (r/r_0), \tag{4}$$

where u_0 is the amplitude of the Fourier component of the speed of the pulsating surface and $k = \omega/V_{\rm fast} = 2\pi/\lambda$ is the wave number. In the low-frequency range, where $(kr_0)^2 = (2\pi r_0/\lambda)^2 \ll 1$, it follows from Equation 4 that

$$u = a_0 r_0^2 / \left(r V_{\rm fast}\right). \tag{5}$$

Here $a_0 = \omega u_0$ is the amplitude of the Fourier component of the acceleration of the pulsating surface. It follows from Equation 5 that the amplitudes of large-scale disturbances, $\lambda > 2\pi r_0$, are entirely determined by the area and acceleration of the emitter surface and not by its speed. In turn, $4\pi a_0 r_0^2 = {\rm d}^2W/{\rm d}t^2 \equiv \ddot{W}$, where W is the volume of the pulsating sphere. The relation $u \propto \ddot{W}$ in the approximation $(kr_0)^2 \ll 1$ holds regardless of the shape of the body with volume W and size r_0 (Landau and Lifshitz, 1987). We therefore have come to the conclusion that the generation of strong wave disturbances is associated exactly with the maximum-acceleration phase of erupting structures.

Equation 5 also holds for $kr_0 = 1$, when the wavelength is equal to the emitter perimeter. Here, the $\sqrt{2}$ factor appears in the denominator of Equation 5. Expressing acceleration a_0 vs. the displacement amplitude $\xi_0 = a_0/\omega^2$, we get

$$u = V_{\rm fast}(2\pi r_0/\lambda)^2(\xi_0/r). \tag{6}$$

If the characteristic size [λ] of the wave is comparable with the emitter perimeter $2\pi r_0$, then the wave amplitude at a distance r from the emitter is

$$u = V_{\rm fast}(\xi_0/r). \tag{7}$$

For filament eruptions from active regions, the typical displacement [ξ_0] in Equation 7 is comparable to the size r_0 of erupting structures at the end of

the impulsive acceleration, $\xi_0/r_0 \approx 1$. The amplitude of the plasma velocity in the resulting wave is comparable with $V_{\rm fast}$ at this time. A question arises of how large are radial displacements $[\xi_0]$ of the surfaces of flare arcades. One can assume an extreme possibility when ξ_0 is comparable to the diameter $[d]$ of the arcade loops, or is comparable to the thickness $[D]$ of the quasi-separatrix surface bound with the current sheet that comprises the arcade. The value of D is comparable to the thickness of expanding flare ribbons. It is convenient to represent Equation 7 as $u = V_{\rm fast}(\xi_0/r_0)(r_0/r)$, where ξ_0 is equal to either d or D, and r_0 is the characteristic size of the arcade. Unlike the previous example, here $\xi_0/r_0 \ll 1$ and the generation of an intense wave is impossible.

All of these circumstances prevent the flare-generation of blast waves and explain the statistical independence of the EUV wave occurrence on the flare size (Long et al., 2017). They also explain why shock waves are not observed in association with confined flares, which are not accompanied by any kind of eruption or rapid expansion of coronal structures (e.g. Thalmann et al., 2015).

2.4. Type-II Bursts

To produce a narrow-band harmonic Type-II emission, its source should be compact. This is possible if it is located in a narrow structure such a coronal streamer (Uralova and Uralov, 1994; Reiner et al., 2003; Mancuso and Raymond, 2004); otherwise, a drifting continuum is expected (Knock and Cairns, 2005). When crossing a streamer, the shock causes in its current sheet a flare-like process that runs along the streamer and produces the Type-II emission. Its source can be located either in a remote streamer(s) hit by an oblique or quasi-perpendicular shock or in the streamer above the parent active region hit by a quasi-parallel shock. The former situation with a compact meter-wave source at a shock flank seems to be typical (Feng et al., 2013; Chen et al., 2014; Alissandrakis et al., 2021). In the less frequent latter case, the Type-II source is located ahead of the CME (Bain et al., 2012; Zimovets et al., 2012; Grechnev et al., 2014). In either situation, a Type-II burst can only start when the shock reaches a streamer.

To analyze Type-II bursts, we plot their expected trajectories on top of the dynamic spectrum and, by adjusting their parameters, fit them to Type-II bands. To calculate their trajectories, we choose a reference point on a band visible on the dynamic spectrum that has a harmonic number $[N_{\rm ref}]$ (1 or 2) at a frequency $f_{\rm ref}$ and time t_1. We find the density from the plasma frequency

$$f = 9 \times 10^3 n^{1/2}, \tag{8}$$

and use the density model described by Equation 1. With a starting estimate of δ, the plasma density in the Type-II source is $n_1 = [f_{\rm ref}(t_1)N_{\rm ref}^{-1}/(9 \times 10^3)]^2$ and its height at t_1 is $x_1 = h_0\,(n_0/n_1)^{1/\delta}$. The height–time plot is calculated from Equation 3 and the density variation is $n(t) = n_0\,[x(t)/h_0]^{-\delta}$. The trajectory of the fundamental-emission band is $f_{\rm fund}(t) = 9 \times 10^3[n(t)]^{1/2}$ and that of the and harmonic band is $f_{\rm harm}(t) = 2f_{\rm fund}(t)$. By adjusting δ and t_0 in sequential attempts, we approach the best-fit trajectories (Grechnev et al., 2011a). The uncertainty of t_0 is typically about $\pm$30 seconds. The wave onset time $[t_0]$ should

be close to the estimate from the images of the eruption observed around this time. The estimate of δ may differ from the measurements of the wave propagation in images due to different plasma-density distributions in the streamer and surrounding corona, as well as different propagation directions. A constant density multiplier does not affect the Type-II trajectory, and the spectrum can be reconciled with measured heights by adjusting n_0, as usually done.

3. Event 1: Shock Wave Associated with a "Ballistic" CME

An unusual 24 December 1996 event (C2.1 GOES importance) was presented by Magdalenić et al. (2008, 2010). Figure 1 summarizes the observational indications revealed by the authors mainly from data of the *Extreme-Ultraviolet Imaging Telescope* (EIT: Delaboudinière et al., 1995), the *Large Angle Spectroscopic Coronagraph* (LASCO: Brueckner et al., 1995), both on board the *Solar and Heliospheric Observatory* (SOHO: Domingo, Fleck, and Poland, 1995).

The SOHO/EIT difference image in Figure 1a shows a suggestion of a rising CME as a faint loop-like structure within the yellow-dashed ellipse. Figure 1b shows the SXR flare emission. The CME height–time plot (black) in Figure 1c combines measurements from EIT, LASCO-C1, and -C2 observations. We used LASCO-C2 data from the online CME catalog of the *Coordinated Data Analysis Workshop* (CDAW) (cdaw.gsfc.nasa.gov/CME_list/: Yashiro et al., 2004), while Magdalenić et al. (2008) got similar results from their own measurements. Figure 1c also shows the derivative of the GOES 0.5–4 Å flux (blue) in comparison with an apparent CME acceleration (green triangle). The event produced a shock wave, as evidenced by a Type-II burst observed within the shaded interval.

The shock speed estimated by the authors from the Type-II burst and the images of its source was $\approx 1100\,\mathrm{km\,s^{-1}}$, whereas the CME speed they estimated around the Type-II onset was as low as $\approx 110\,\mathrm{km\,s^{-1}}$ (the oblique dash-dotted line in Figure 1c). The mismatch rules out the bow-shock excitation. Magdalenić et al. (2010) compared these results to the analytical model developed by Žic et al. (2008) of the shock-wave formation by an impulsively expanding three-dimensional piston. The modeling showed that with the acceleration phase denoted by the green triangle in Figure 1c (and down to five minutes) and the CME speed increasing up to $250\,\mathrm{km\,s^{-1}}$ in this interval (with an average speed being close to the estimated $110\,\mathrm{km\,s^{-1}}$), the shock-formation time was as long as 37 (down to 18) minutes. With these parameters, the shock could not appear as early as the Type-II burst started. The authors concluded that the CME was unlikely to be the driver of the shock wave and came to its flare-related origin.

We will try to figure out what happened in this unusual event. First of all, the CME kinematics presented in Figure 1c looks strange for the following reasons:

i) The sudden transition from gradual acceleration to deceleration is incomprehensible. The CME may slow down due to a collision with something, but no images support this assumption. Another reason for the CME slowing down could be reconnection between its magnetic structure and the environment, but no signs of this are observed in X-rays.

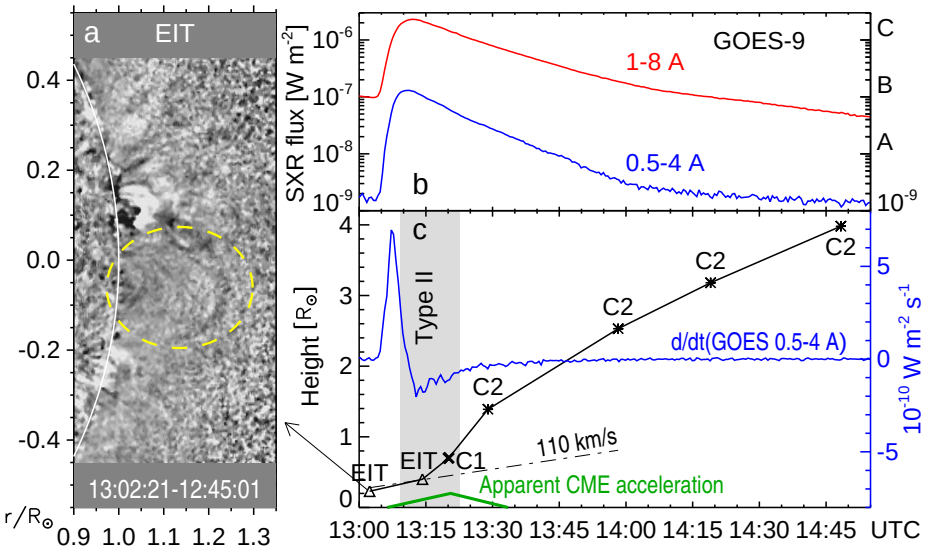

Figure 1. Overview of the 24 December 1996 event according to the findings of Magdalenić et al. (2008, 2010). **a**) Indication of the CME appearance at 13:02:21 in the SOHO/EIT 195 Å difference image (dark loop-like features within the *yellow-dashed ellipse*). The *axes* show the distances from solar disk center in solar radii. **b**) SXR fluxes recorded in two GOES-9 channels. **c**) CME height–time plot (*black*) based on measurements from EIT (*triangles*), LASCO-C1 (*slanted cross*), and LASCO-C2 (*asterisks*) along with a derivative of the 0.5–4 Å flux (*blue*) and apparent CME acceleration (*green triangle*). The first EIT point corresponds to panel **a**, as the *arrow* indicates. The *shading* denotes the interval of the Type-II burst. The *oblique dash-dotted line* corresponds to the speed of 110 km s^{-1} estimated by Magdalenić et al. (2010).

ii) Although Maričić et al. (2007) reported some events with a considerable mismatch between the CME acceleration phase and the rise phase of the SXR emission, this situation is unusual and requires special investigation.

The strange shape of the CME height–time plot is determined by the first EIT point at 13:02 (*all times henceforth are referred to UTC*). We investigate the situation using the variance analysis (Nindos et al., 2002; Grechnev, 2003). The variance (or standard deviation) is calculated along each pixel in the data cube. Variable objects appear on the variance map as bright features. Figures 2a and 2b show the negatives of the variance maps computed from EIT image sets observed before the eruption and after it. The eruption itself is clearly visible in Figures 2c (EIT) and 2d (LASCO-C1). Comparison of the features inside the yellow-dashed ellipses in Figures 2a and 2b does not reveal any significant changes from 12:12 through 13:02. Hence, the loop-like feature visible in Figure 1a was most likely due to minor motions of nearly static coronal loops.

To find the probable onset time of the shock wave, we consider the Type-II burst recorded by the spectrographs of the Astrophysical Institute Potsdam (AIP) that is shown in Figure 3. The blue-dashed trajectories plotted on top of the dynamic spectrum were calculated using the technique described in Section 2.4 with $\delta = 2.60$ and the wave onset time $t_0 =$13:04:40, whose probable uncertainty is within $\pm$1 minute. The second, weaker Type-II burst may be

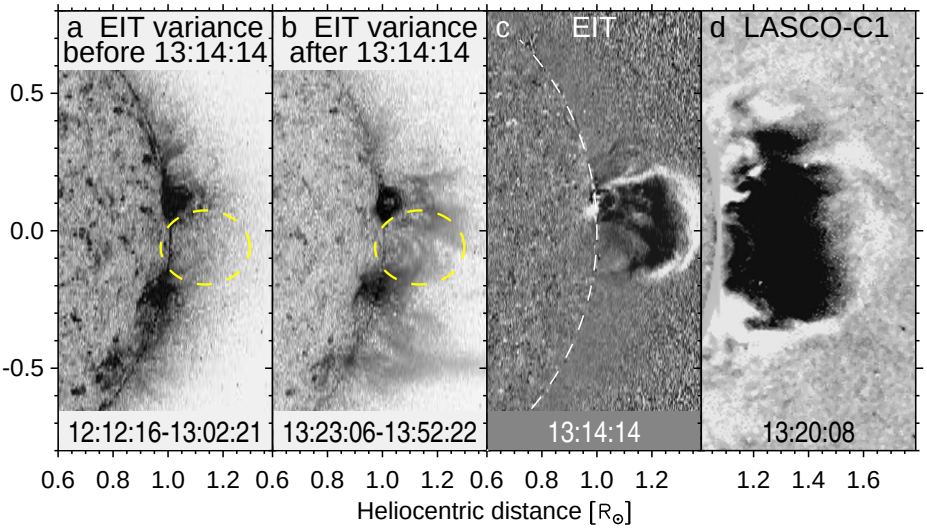

Figure 2. Negative variance maps computed from EIT 195 Å images observed before the clear CME appearance (**a**, 12:12:16 – 13:02:21) and after it (**b**, 13:23:06 – 13:52:22). The *yellow-dashed ellipses* outline the area of the presumable CME appearance in Figure 1a. **c**) Conspicuous CME appearance in the EIT 195 Å difference image at 13:14:14. **d**) The CME visible in the LASCO-C1 difference image at 13:20:04.

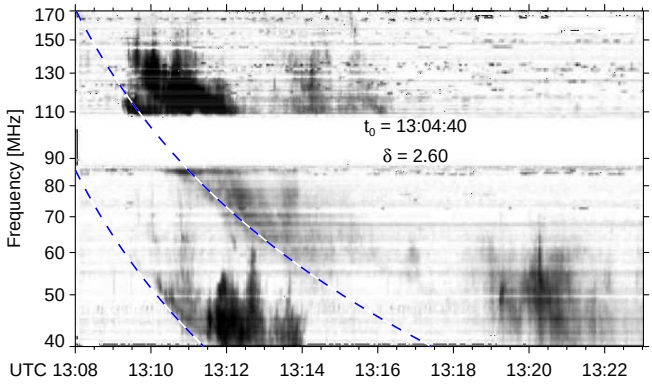

Figure 3. Type II burst recorded on 24 December 1996 by the AIP spectrographs (adapted from Magdalenić et al., 2008) along with the *blue-dashed* trajectories calculated for an impulsively excited piston shock with an onset time $t_0 = 13{:}04{:}40$ and $\delta = 2.60$.

associated with the passage of a reflected wave, but it is difficult to determine its cause due to insufficient data. The second Type-II burst does not affect the estimated wave onset time, which practically falls into the flare impulse phase (cf. the derivative of the 0.5 – 4 Å flux in Figure 1c). This result is consistent with the conclusions of Magdalenić et al. (2008, 2010).

To elucidate the subsequent evolution of the CME and shock wave, we consider their manifestations in white-light images produced by LASCO. Figure 4 presents the CME body and wave traces observed in LASCO-C2 and -C3 images. A nice finding of Magdalenić et al. (2008) is the wave manifestation in the

deflection of a coronal ray visible in running-difference images (e.g. the northernmost bright feature in Figures 4b and 4c). The CME body was well behind the wave front, but it is difficult to reliably identify them in the same images. We therefore consider two image sets. Heavily contrasted running-difference images in Figures 4a–4f (upper row) reveal the wave traces. Figures 4m and 4n on the right show two C3 images, where they are still detectable. Moderately contrasted non-subtracted images in Figures 4g–4l (lower row) present the helical CME body. A southern extended bright feature is another coronal ray, as comparison of the two rows indicates. The blue arcs outline the leading edge of the CME body and the green arcs outline the wave manifestations in the deflections of coronal rays. The radii of the arcs were calculated analytically based on initial manual estimates; the parameters of the fit were adjusted in sequential attempts.

The kinematics of the wave front was calculated using the technique described in Section 2.2 from Equation 3. We used the wave onset time $t_0 = 13{:}04{:}40$ estimated from the Type-II burst and adjusted δ iteratively. The slanted crosses (same in both rows) represent the measurements from the online CDAW CME catalog (cdaw.gsfc.nasa.gov/CME_list/). The bright features measured in this event were located between the wave front and CME body.

To follow the expansion of the CME body, we combined the speed–time dependencies of the initial impulsive Gaussian acceleration and the subsequent self-similar expansion that resulted from a joint action of magnetic forces, plasma pressure, and gravity (Low, 1982; Uralov, Grechnev, and Hudson, 2005). The formulas for the self-similar kinematics can be found in Grechnev et al. (2014).

We required for the initial phase: i) The initial CME speed is zero and its final speed at the end of the acceleration phase noticeably exceeds the speed at $1\,\mathrm{R}_\odot$ estimated in the CDAW CME catalog from the second-order fit ($340\,\mathrm{km\,s^{-1}}$) to ensure deceleration of the CME in LASCO images. ii) The rise of the speed–time plot resembles the rise of the SXR flux (Zhang et al., 2001; Maričić et al., 2007). iii) The acceleration pulse resembles the microwave burst and the derivative of the SXR flux and can lead them by up to two minutes (Temmer et al., 2008, 2010; Grechnev et al., 2013, 2015, 2016). The subsequent self-similar motion was calculated by adjusting its parameters to match the decelerating CME expansion in LASCO images. After combining the speeds calculated for the initial acceleration phase and subsequent self-similar expansion, the temporal dependencies for the distance and acceleration were computed by numerically integrating and differentiating the resulting speed–time dependence, respectively. The parameters of the fitting dependencies were finally refined in this way.

Figure 5 presents the reconstructed kinematic plots for the CME and wave. We ignored the EIT data point at 13:02 that is most likely spurious. The kinematic plots do not exhibit any peculiarities. Figure 5a shows the distance–time plots for the CME body and wave along with the measurements from the CME catalog. The origins of the CME and wave are at solar limb. The open circles in Figure 5a correspond to the green arcs outlining the wave traces in Figure 4 and the squares correspond to the blue arcs outlining the CME body. The pink dot represents the height of the Type-II source at 164 MHz estimated by Magdalenić et al. (2008, 2010). The dash-dotted line indicates the wave onset time.

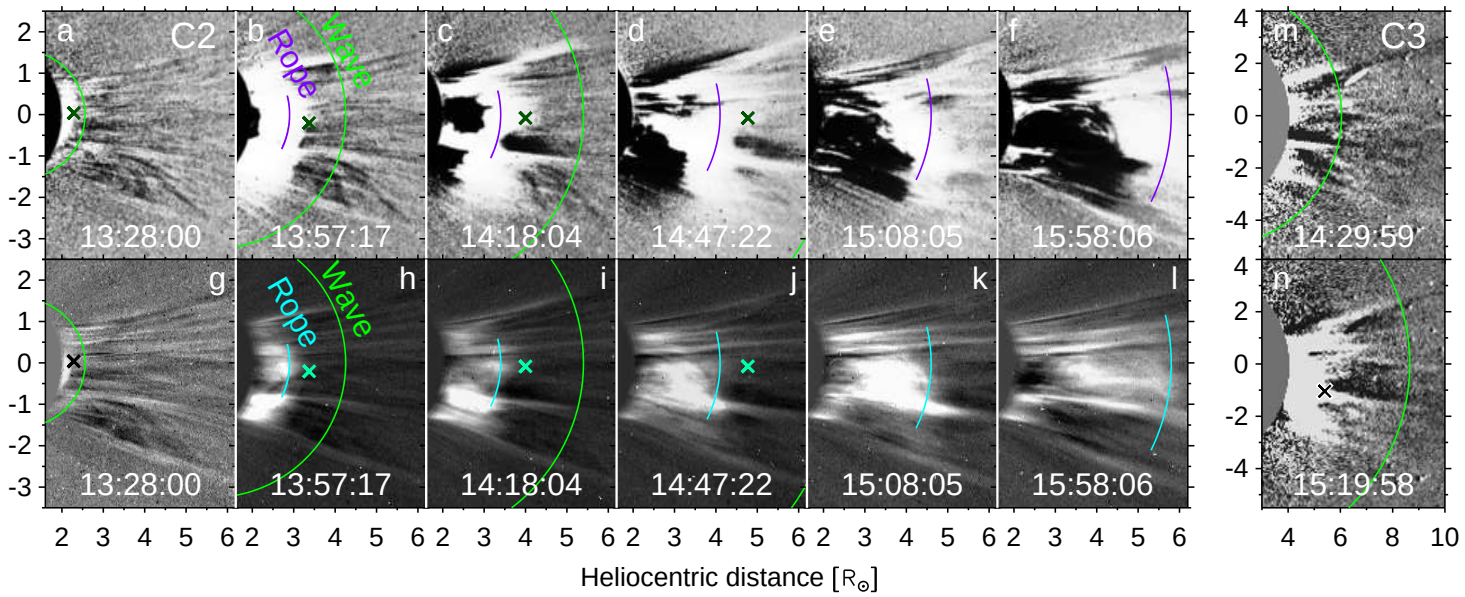

Figure 4. CME body and wave trace observed in LASCO images on 24 December 1996: **a**–**f**) wave trace in enhanced-contrast C2 running-difference images; **g**–**l**) CME body in non-subtracted C2 images; **m**, **n**) wave trace in enhanced-contrast C3 running-difference images. The *blue arcs* denoted "Rope" outline the clearly visible part of the flux-rope CME body. The *green arcs* denoted "Wave" outline the wave trace. The *slanted crosses* represent the measurements from the CME catalog where they are available (four left pairs of C2 images and the lower C3 image). The *axes* show the distances from solar disk center measured in solar radii.

To match the wave traces in Figure 4, we used $\delta = 2.79$ that is slightly different from $\delta = 2.60$ found for the Type-II burst. The difference can be due to different propagation directions of the projected shock-wave traces in Figure 4 and the actual Type-II source, which could be located in an off-plane streamer.

Figure 5b presents the speed–time plots for the CME body and shock wave along with the 0.5–4 Å GOES flux. The shading indicates when the Type-II burst was observed. The wave speed at its onset was $800\,\mathrm{km\,s^{-1}}$, i.e. lower, but comparable with $1100\,\mathrm{km\,s^{-1}}$ estimated by Magdalenić et al. (2010) in a complex way. The CME speed at the shock onset time was $580\,\mathrm{km\,s^{-1}}$, i.e. about twice as high as the maximum speed of $250\,\mathrm{km\,s^{-1}}$ of the impulsive piston considered by Magdalenić et al. (2010) in their modeling.

Figure 5c presents the acceleration–time plot of the CME body in comparison with the derivative of the SXR flux. The inset (Figure 5d) shows its expanded initial part and a microwave burst at 2.7 GHz (Sagamore Hill) that is noisy because of the low flux and insufficient sensitivity of the radiometer. The acceleration pulse is similar to both the SXR-flux derivative and the microwave burst. The half-height duration of the acceleration pulse is 2.3 minutes, i.e. about half the minimum duration of five minutes considered by Magdalenić et al. (2010) in their modeling. The acceleration pulse up to $4.5\,\mathrm{km\,s^{-2}}$ is followed by deceleration up to $-500\,\mathrm{m\,s^{-2}}$ that has a long decreasing tail. For comparison, Figure 5d also shows the plasma pressure variations (pink) $p = 2kT\,(\mathrm{EM}/V)^{1/2}$ (with $[k]$ being the Boltzmann constant) estimated from the temperature $[T]$ and emission measure [EM], which were calculated from the SXR GOES fluxes. The unknown volume $[V]$ of the SXR-emitting source was assumed to be invariable. As the plot demonstrates, at the moment of the shock-wave onset, the pressure just started to rise and increased more smoothly than the sharp acceleration pulse.

The estimates of the acceleration, its duration, and CME speed at the end of the acceleration phase are all within the ranges that are expected and actually observed in flare-associated eruptions (e.g. Green et al., 2018; Grechnev et al., 2013, 2016, 2019). With these parameters and the acceleration peak time around 13:05, the appearance of an impulsively-excited piston shock at about 13:09 is not challenging even in the approximation adopted in the Žic et al. (2008) model.

Interestingly, the decreasing CME speed corresponds to a free-fall ("ballistic") motion of a body governed by gravitational deceleration. From the potential plus kinetic energy conservation it follows that

$$v_1^2 - v_2^2 = 2G\mathrm{M}_\odot\,(1/r_1 - 1/r_2)\,, \tag{9}$$

where v_i is the speed of the body at a distance r_i, G is the gravitational constant, and $\mathrm{M}_\odot$ is the mass of the Sun. For the CME distance and speed at the end of the plot in Figure 5 (16:00:00), we estimate $v_2 = 217\,\mathrm{km\,s^{-1}}$ at $r_2 = 5.61\,\mathrm{R}_\odot$. For an earlier time of 13:20:00 (close to the LASCO-C1 observation), we estimate from our fit $v_1 = 451\,\mathrm{km\,s^{-1}}$ at $r_1 = 1.72\,\mathrm{R}_\odot$. For a purely free-fall motion, the CME speed at this distance $v_{1\mathrm{G}} = 449\,\mathrm{km\,s^{-1}}$ practically coincides with our fit. Even as low as in the low corona, the CME moved in the free-fall regime.

The wave-to-CME speed ratio at the deceleration stage was nearly constant at least until the end of the Type-II burst; i.e. the expansion was close to being

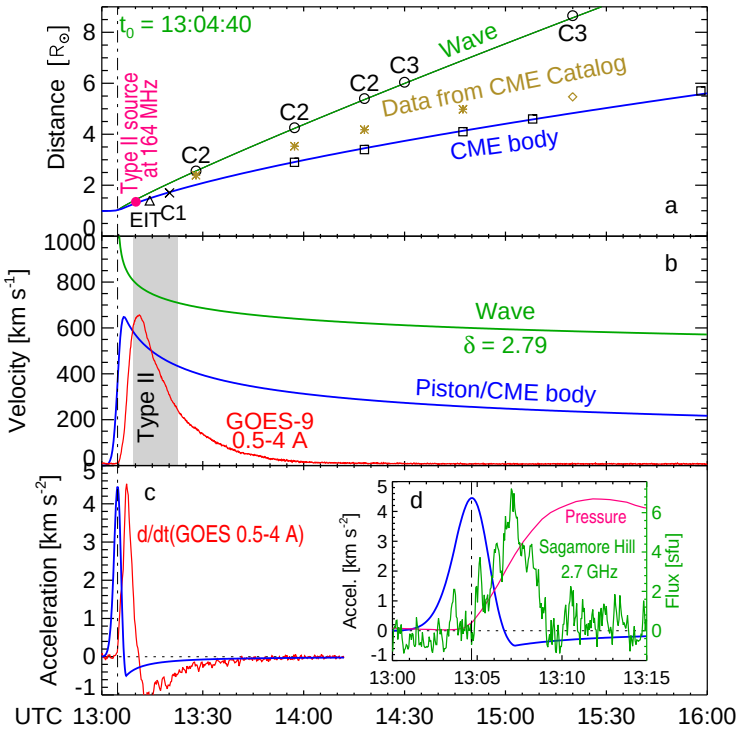

Figure 5. Reconstructed kinematics of the CME body (*blue*) and wave (*green*) in the 24 December 1996 event. **a**) Distance–time plots based on our measurements (*black symbols*). The *pink dot* represents the position of the Type-II source according to Magdalenić et al. (2008, 2010). The *brown symbols* represent the measurements from the CME catalog. **b**) Velocity—time plots along with the GOES-9 flux in the 0.5–4 Å channel (*red*). The *shading* indicates the interval when the Type-II burst was observed. **c**) Acceleration–time plot along with a derivative of the 0.5–4 Å GOES-9 flux (*red*). **d**) The *inset* shows an expanded initial part of the acceleration pulse in comparison with a microwave flux at 2.7 GHz (*green*) and plasma pressure computed from GOES-9 data (*pink*, arbitrary units). The *vertical dash-dotted line* in all panels marks the probable wave onset time $t_0 = 13{:}04{:}40$.

self-similar. This is typical of piston shocks (Uralov, Grechnev, and Ivanukin, 2019), as opposed to blast waves. Then the wave speed decreased, approaching the fast-mode speed in the environment (cf. the model by Mann et al., 2003). The shock decayed that led to the termination of the Type-II burst.

To summarize, revisiting the challenging 24 December 1996 event revealed observational problems that made it difficult to understand what actually happened in this event. Those are in particular the deceptive EIT observation at 13:02 and complications in the separation of CME and wave signatures in LASCO images. Our analysis confirms the conclusions of Magdalenić et al. (2008, 2010) that the shock wave in this event was impulsively excited and it was not a bow shock. The shock wave really resembled a hypothetical flare-generated decelerating blast wave; however, the delayed smooth increase in the flare pressure and nearly self-similar expansion of the shock wave and the CME body are incompatible with this assumption. The reconstructed kinematics of the CME body and the

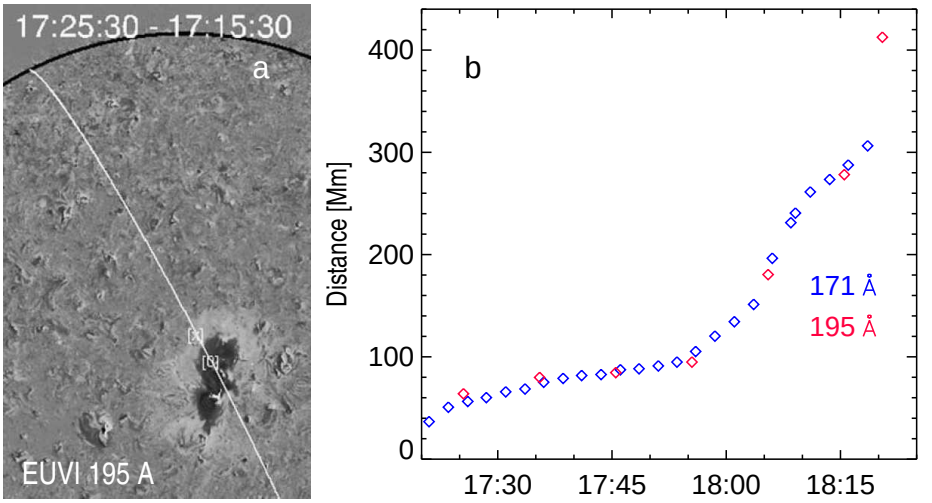

Figure 6. Overview of the 8 December 2007 event as considered by Zhukov, Rodriguez, and de Patoul (2009) (adapted from their figures). **a**) A part of the STEREO-A/EUVI 195 Å difference image with a faint bright EUV wave and the great circle (*white*) on the solar surface, along which the distances were measured. The *black arc* denotes solar limb. **b**) Distance–time plot of the EUV wave propagation measured from the EUVI 195 Å (*red symbols*) and 171 Å (*blue symbols*) images along the great circle shown in panel **a**.

shock wave removes the contradiction between the apparent manifestations that mimic a flare blast wave and the theoretical difficulties faced by this hypothesis (Section 2.3). The kinematic characteristics fully correspond to a piston shock impulsively excited by a sharply accelerating CME or its internal structure.

4. Event 2: EUV Disturbances with Challenging Kinematics

Zhukov, Rodriguez, and de Patoul (2009) presented an intriguing event observed by the STEREO's *Extreme Ultraviolet Imager* (EUVI) on 8 December 2007. The event occurred in a plage region without sunspots 10977 located at S06 W26 as seen from the Earth's direction, at S07 W47 for STEREO-B, and at S06W04 for STEREO-A. Most likely, there was no Type-II burst, while a Type-III burst was recorded from 16 to 0.1 MHz starting at 17:15 (swaves.gsfc.nasa.gov/).

Zhukov, Rodriguez, and de Patoul (2009) revealed in this event EUV disturbances with challenging kinematics shown in Figure 6. The authors concluded that these disturbances were not of a wave nature, being instead due to changes in magnetic fields caused by the CME eruption. To explain the strange shape of the distance–time plot, they proposed that the erupting system temporarily slowed down and nearly stopped at a certain height and then completely erupted. Warmuth and Mann (2011) also stated that the characteristics of this event were markedly different from other events that they considered.

The presence of two increasing parts in the distance–time plot (except for the last 195 Å point), one starting around 17:20 and the other after 17:55, suggest that two successive eruptions occurred in this region. This guess is confirmed

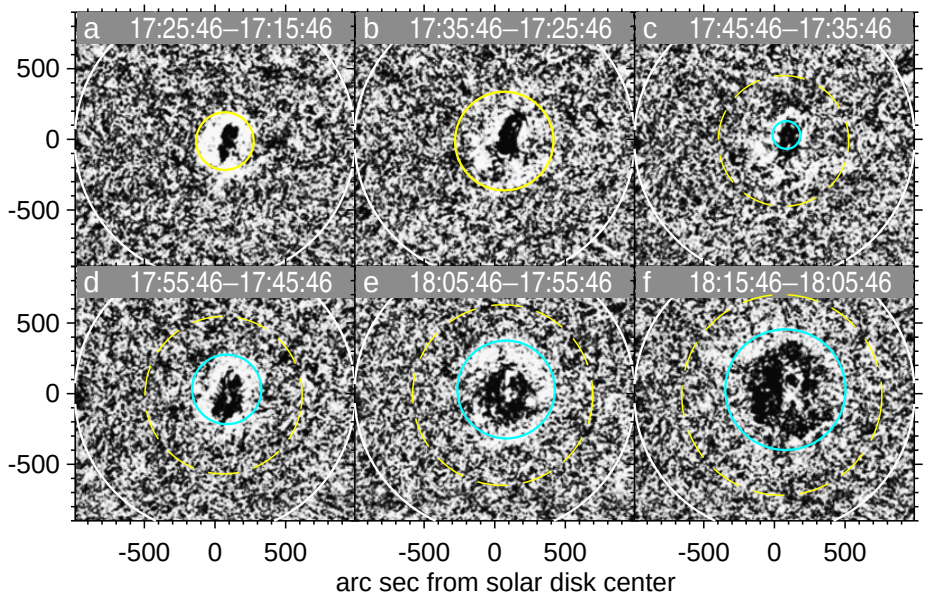

Figure 7. Two consecutive magnetosonic EUV waves revealed from STEREO-A/EUVI 195 Å difference images on 8 December 2007. The *yellow* and *blue* ellipses represent the wave fronts calculated for an isotropic wave propagation. The *thick-solid ellipses* outline the observed EUV waves and the *thin-dashed ellipses* represent their expected positions afterwards. The *white circle* denotes solar limb.

by the STEREO A+B COR1RD movie for that day at cdaw.gsfc.nasa.gov/stereo/daily_movies/. Indeed, the images from the inner STEREO-B/COR1 coronagraph show above region 10977 a narrow spray-like ejection at 17:45 and 18:05; and then, starting at 18:35, a broader and brighter, well-structured CME appeared.

Using these indications, we revealed two faster, weaker EUV disturbances in STEREO-A/EUVI difference images in the 195 Å channel that is more sensitive to EUV waves than the lower-temperature 171 Å channel. Figure 7 and the 2007-12-08_EUVI_wave.mpg movie in the Electronic Supplementary Material present the two EUV waves along with the ellipses calculated using Equation 3 for their expected propagation in an isotropic corona. The yellow ellipse with $t_{01} = 17{:}18{:}00$ outlines the first EUV wave and the blue ellipse with $t_{02} = 17{:}43{:}00$ outlines the second EUV wave. The apparent "contraction" of the EUV brightening between Figures 7b and 7c is due to the appearance of the second EUV wave, while the first, broader EUV wave disappeared.

Given the known times $[t_{01}]$ and $[t_{02}]$ of the presumable eruptions that excited the EUV waves, it is possible to reconstruct the height–time plots for the two mass ejections observed by STEREO-B/COR1. The thin-gray symbols and bars in Figure 8 represent our measurements with uncertainties. The first spray-like ejection visible in two images looks like dispersed remnants of an eruptive filament that disintegrated in reconnection with surrounding magnetic fields. Being not united by a common magnetic field, the remnants scattered, lost brightness, and disappeared in the third COR1 image. We measured for the spray-like ejection the height of its thick middle part rather than the leading

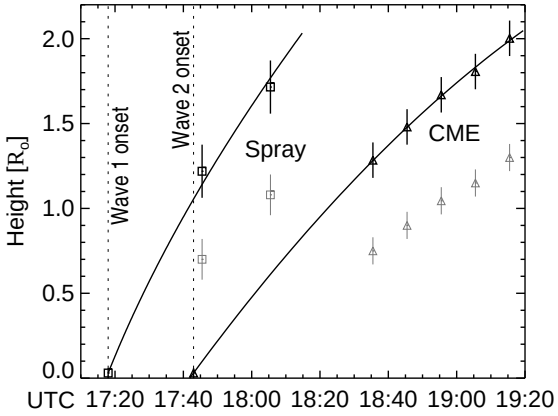

Figure 8. Height–time plots of two mass ejections observed by STEREO-B/COR1 on 8 December 2007. The *symbols* and *bars* represent our measurements with uncertainties (*thin-gray*) and those corrected to the radial direction (*thick-black*). The *solid curve* for the spray corresponds to the free-fall motion (Equation 9). The *solid curve* for the CME is a second-order fit of the measurements. The *vertical dotted lines* mark the onset times of the two EUV waves.

edge. Because this ejection is expected to move in the free-fall regime as long as it is not confined by tops of loops, its kinematics should refer to real distances from the Sun's center rather than to their plane-of-the-sky projections.

The real heliocentric distance $[r]$ was found as $r = r_{\rm obs}/\sin\theta$, where $[r_{\rm obs}]$ is the observed projection and $\theta \approx 50^\circ$ is the angle with a vertex in the Sun's center between the line of sight and the axis of the ejection. The corrected height-time measurements for both ejections are shown in Figure 8 with thick-black symbols; for the second ejection (CME) we measured the leading edge of its bright frontal structure. The initial heights of 20 Mm were assumed in both cases.

The height–time plot of the spray-like ejection was calculated for the free-fall motion with an initial speed of $590\,{\rm km\,s^{-1}}$ at 20 Mm. Its onset time is close to that of the Type-III burst. The height–time plot of the CME is the second-order fit of the measurements that is easier to use than the self-similar fit. The difference between the trajectories that the two methods provide is $< 2\,\%$ within the range shown in Figure 8. The initial speed of the CME was 320–340 $\rm km\,s^{-1}$. The trajectories of the two mass ejections confirm their association with the eruptions that produced the two EUV waves. To reach the initial speed, an impulsive acceleration is required. After that, both ejections only decelerated.

To find the possible sources of the fast EUV waves, Figure 9 shows STEREO-A/EUVI 171 Å images. The 2007-12-08_EUVI_171_eruptions.mpg movie in the Electronic Supplementary Material shows them in more detail. Figure 9a presents a dark filament. The green contour outlines its southern part R1. The filament got brighter in Figure 9b, erupted and became a twisted feature in Figure 9c that could be either an expanding flux rope or its transformation into a jet in reconnection with the surrounding magnetic field, which looks more likely. The eruption produced wave-like disturbances that caused the motions of coronal loops visible in the movie. Figure 9d shows the situation between the two eruptions. Manifestations of the second eruption are inconspicuous. Motions of faint

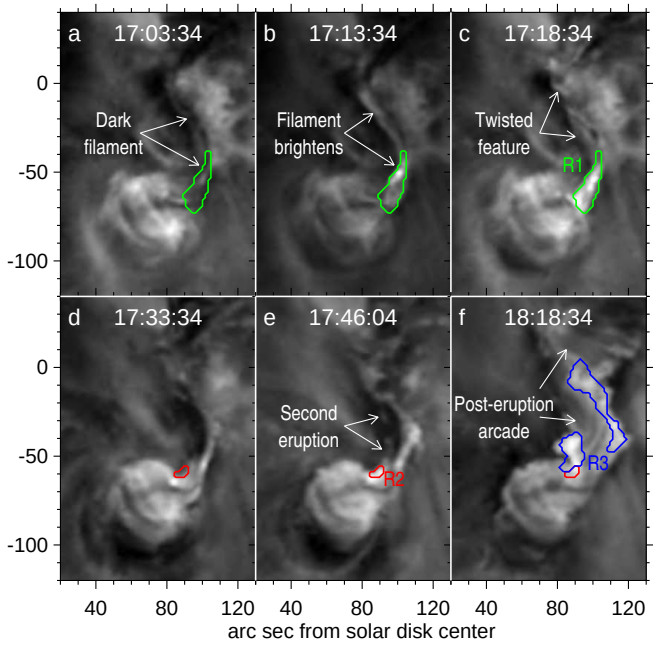

Figure 9. Manifestations of two eruptions in the 8 December 2007 event in STEREO-A/EUVI 171 Å images. **a**–**c**: first eruption (*top*), **d**–**f**: second eruption (*bottom*). The *colored contours* outline characteristic features R1, R2, and R3, whose temporal profiles are shown in Figure 10.

features indicated by the arrows in Figure 9e are detectable between 17:38 and 17:48. After 17:53, the post-eruption arcade visible in Figure 9f developed.

Figure 10 shows the temporal relations between the eruptions and EUV disturbances. The temporal profiles of the average brightness of characteristic features R1, R2, and R3 in Figure 10a were computed from the STEREO-A/EUVI 171 Å images, in which solar rotation was compensated for. Figure 10b presents SXR GOES fluxes. Figure 10c shows the distance–time plots of the two EUV waves, whose onset times $[t_{01}]$ and $[t_{02}]$ are denoted by the vertical dotted lines, and Figure 10d shows their speed–time plots.

Figure 10a indicates two distinct eruptions. The first EUV wave appeared during the first eruption that did not manifest in soft X-rays, as Figure 10b shows. The first part of the whole event until about 17:40 was one of the weakest events, in which an EUV wave was detected (cf. Nitta et al., 2013). The first eruption was followed by the development of dimming. Then, the next eruption occurred and produced the second EUV wave at about 17:43. After the second eruption, an arcade developed, whose SXR emission was as low as A8.3. The marginal GOES importance of the event was apparently determined by very weak magnetic fields in the source region without sunspots.

The symbols in Figure 10c represent the Zhukov, Rodriguez, and de Patoul (2009) data. The curves represent our measurements of the two fast EUV waves (Figure 7). The onset times of the first fast EUV wave and the slower EUV disturbance found by the authors practically coincide. The first EUV wave visible in Figures 7a and 7b ran far ahead with a speed decreasing from about 210 to

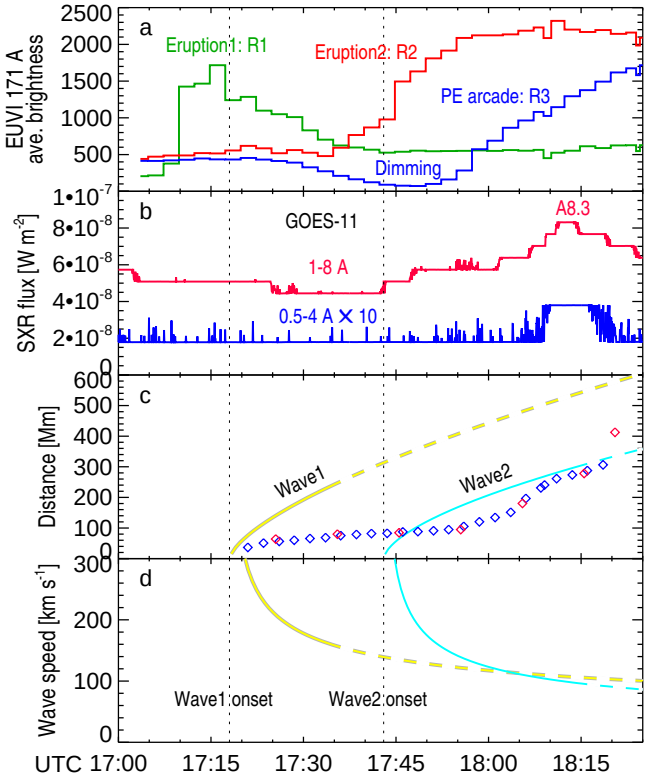

Figure 10. Temporal profiles characterizing the two eruptions and EUV disturbances in the 8 December 2007 event. **a**) Average brightness over the *contoured regions* in Figure 9 plotted with the *corresponding colors*. **b**) Soft X-ray fluxes in two GOES channels. The 0.5–4 Å flux is magnified by a factor of ten. **c**) Distance–time plots of the two magnetosonic EUV waves presented in Figure 7 in comparison with the measurements of Zhukov, Rodriguez, and de Patoul (2009) presented in Figure 6b. **d**) Speed–time plots of the two magnetosonic EUV waves. The *dashed portions* of the plots in panels **c** and **d** are not observed.

160 km s^{-1} at the corresponding times (Figure 10d). The speed of the slower disturbance estimated by the authors in this interval was as low as 20–30 km s^{-1}. The second EUV wave appeared well before the second increase in the distance–time plot measured by the authors; nevertheless, the two measurements are close to each other between 18:08 and 18:18. The last measurement in 195 Å that looks as an outlier may be a late signature of the passage of the first EUV wave.

To understand the relationship between the Zhukov, Rodriguez, and de Patoul (2009) and our measurements, Figure 11 presents a set of EUVI 171 Å difference images along with the yellow and blue ellipses corresponding to the outermost manifestations of the two fast EUV waves shown in Figure 7. The short green arcs represent the measurements of the authors along the white great circle.

The dimming around the eruption site is elongated in the SSE–NNW direction. The dimmed region in Figures 11a and 11b is surrounded by a relatively bright border, whose outermost edges are close to the yellow ellipse that outlines the first fast EUV wave. Then, the dimming and the border slowly expand in

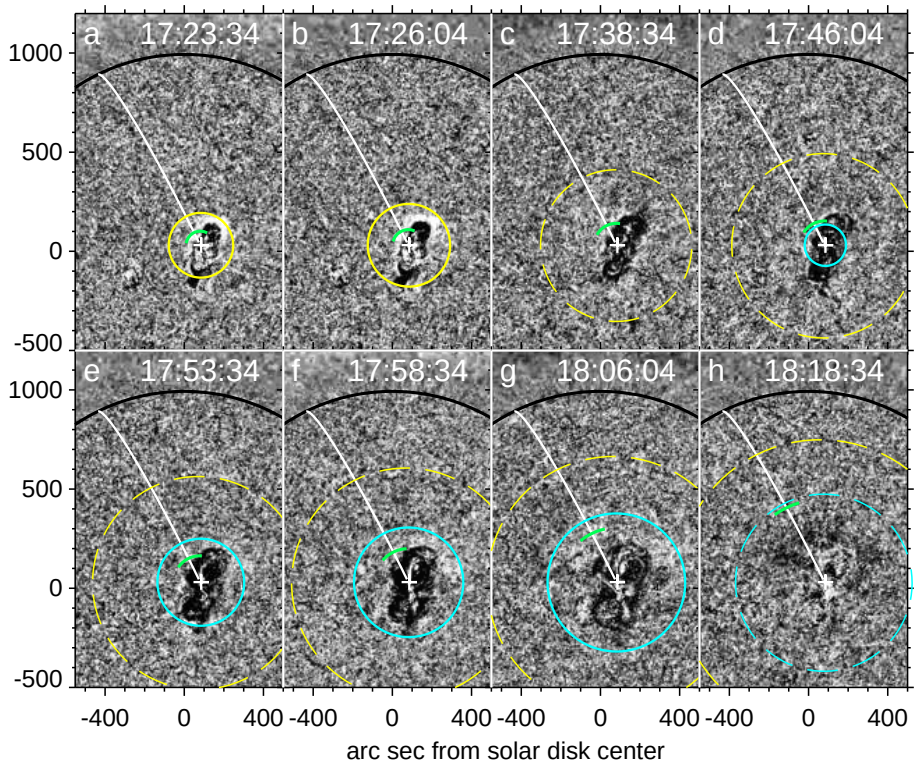

Figure 11. EUV disturbances in STEREO-A/EUVI 171 Å difference images in the 8 December 2007 event. The *yellow* and *blue ellipses* outline the fast EUV waves (same as in Figure 7.) The *short green arcs* represent the Zhukov, Rodriguez, and de Patoul (2009) measurements along a great circle (*white line*, same as in Figure 6a). The *black arc* denotes the limb.

Figures 11c and 11d, while the border becomes faint. The expected position of the first fast EUV wave at that time is far ahead. The measurements of Zhukov, Rodriguez, and de Patoul (2009) refer to a sector of the enhanced-brightness border in the NNE direction, where its size is smaller than in the NNW direction.

We agree with the authors that the slow EUV disturbance they identified after the first eruption was not of a wave nature. The brighter border of the dimming could indeed be due to the field-line-stretching effect, i.e. an increase in the column emission measure caused by the convergence of the legs of loops stretched by the eruption (Chen et al., 2002; Chen, Fang, and Shibata, 2005; Chen and Wu, 2011). However, heating not excluded by Zhukov, Rodriguez, and de Patoul (2009) was unlikely implicated in the brightening visible in the 171 Å channel that is sensitive to radiation from plasma with a temperature of ≈ 1 MK.

Conversely, the two fast EUV waves that we detected were most likely associated with true MHD waves with dome-shaped fronts, whose lower parts were tilted toward the solar surface (Hudson et al., 2003; Grechnev et al., 2011a). A probable cause of an EUV-wave brightening here is an increase in the column emission measure of coronal structures compressed from above by the wave front.

Both fast EUV waves initially were elongated (Figures 7a and 7d); their domes were laterally-flattened ellipsoids that may be due to their exciters and the fast-mode speed distribution. The second EUV wave observed for a longer time later became symmetric (Figures 7e and 7f), suggesting that its dome approached a spheroid. A faint brightening visible in 171 Å (Figures 11f–11h) roughly corresponds to the second fast EUV wave, whose shape gradually changed between 17:55 and 18:10. This interval corresponds to the second increase in the distance–time measurements made by Zhukov, Rodriguez, and de Patoul (2009) that are shown in Figures 6b and 10c. These measurements correspond to the second fast EUV wave between 18:08 and 18:18, when it became more or less symmetric.

In summary, the intriguing distance–time plot of Zhukov, Rodriguez, and de Patoul (2009) was the result of two successive eruptions, each of which produced a fast MHD wave and field-line-stretching effect. The measurements were related to the latter effect after the first eruption and to an MHD wave after the second.

The kinematics of fast EUV waves indicate that the responsible MHD waves were impulsively excited and clearly not by flares. The first eruption was impulsive; its height–time plot and the maximum speed were similar to those in Event 1 (Figure 5, Section 3). The CME caused by the second eruption was too slow to produce a bow shock and its lateral expansion was still slower. In the absence of a Type-II burst, it is difficult to judge if the MHD waves were shock waves or large-amplitude simple waves. The presence of a shock is guaranteed by the presence of a Type-II burst, but its absence does not guarantee the absence of a shock. We do not exclude that shocks were short-lived, and then died out.

5. Concluding Remarks

The two events that we considered demonstrate how complex and perplexing observations can be. Thanks to efforts of Magdalenić et al. (2008, 2010) and Zhukov, Rodriguez, and de Patoul (2009), one has learned about these intriguing events and ideas proposed by the authors to address observational challenges. Revisiting these events has revealed their additional interesting aspects. Our analysis has been facilitated by the use of analytical methods, especially those described in Section 2, and led to the following outcome.

Besides the challenging kinematics and despite conspicuous differences, the events had some similarities. All of the three ejections, which were revealed, impulsively accelerated at the initial stage and only decelerated afterwards. They impulsively excited fast MHD waves, although it is not clear whether or not shocks were formed in the second event, which was extremely weak.

Our consideration of the 24 December 1996 event seems to shed light on other events that Magdalenić et al. (2010) presented as the cases of flare-generated shock waves. The ejections in three out of four these events decelerated, similar to the 24 December 1996 CME. The slightly accelerating ($1.7\,\mathrm{m\,s^{-2}}$) jet-like ejection in the fourth event (9 July 2002) also initially impulsively accelerated. We agree with the authors that the shock waves in these events were excited impulsively and were not bow shocks; however, their flare-related origin is also unlikely. The authors obtained negative results in the modeling of the piston

shock possibly because they underestimated the maximum speeds of the ejections and overestimated the acceleration durations. Also, comparison of the images of a CME and a Type-II source may be complicated by its off-plane position.

The course of the 8 December 2007 event with two successive eruptions that we identified from additional observations looks simpler than the complex rise of an erupting structure, as Zhukov, Rodriguez, and de Patoul (2009) suggested. Eruptions with non-monotonic velocity variations are sometimes really observed, but this was not the case here. The involvement of diverse processes with a similar outcome caused complications that were difficult to untangle. This very weak event also demonstrated the impulsive-piston excitation of a fast MHD wave.

The expansion of the CME in Event 1 and the spray-like ejection in Event 2 was governed by gravity. Since acceleration rather than velocity is decisive for the impulsive shock excitation, a piston shock can appear even if the speed of an ejection is insufficient to produce a CME. Such events are discussed in Article II.

Acknowledgments We thank M. Temmer and J. Magdalenić for useful discussions and all authors of previously published articles that studied the events in question. We are grateful to the anonymous reviewer for useful remarks.

We thank the NASA's STEREO/SECCHI science and instrument teams; the science and instrument teams of EIT and LASCO on SOHO, the US AF RSTN network, and the GOES satellites for the data used here. We are grateful to the team maintaining the CME Catalogs at the CDAW Data Center by NASA and the Catholic University of America in cooperation with the Naval Research Laboratory. SOHO is a project of international cooperation between ESA and NASA.

The analysis and consideration of the 8 December 2007 event, the measurements of fast MHD waves, and discussion of the results was funded by the Russian Science Foundation under grant No. 21-72-00039 (V. Kiselev: Sections 4 and 5). The generalization of basic concepts and methods and the analysis of the 24 December 1996 event were financially supported by the Ministry of Science and Higher Education of the Russian Federation (V. Grechnev, A. Uralov: Sections 2 and 3).

Data Availability

The datasets analyzed during the current study were derived from the following public domain resources:

Virtual Solar Observatory https://sdac.virtualsolar.org/
CDAW Data Center https://cdaw.gsfc.nasa.gov/
SPACE WEATHER PREDICTION CENTER https://www.swpc.noaa.gov/
SOHO LASCO CME CATALOG https://cdaw.gsfc.nasa.gov/CME_list/

Disclosure of Potential Conflicts of Interest

The authors declare that they have no conflicts of interest.

References

Afanasyev, A.N., Uralov, A.M.: 2011, Coronal shock waves, EUV waves, and their relation to CMEs. II. Modeling MHD shock wave propagation along the solar surface, using nonlinear geometrical acoustics. *Solar Phys.* **273**, 479. DOI. ADS.

Afanasyev, A.N., Uralov, A.M., Grechnev, V.V.: 2013, Propagation of a fast magnetoacoustic shock wave in the magnetosphere of an active region. *Astron. Rep.* **57**, 594. DOI. ADS.

Alissandrakis, C.E., Nindos, A., Patsourakos, S., Hillaris, A.: 2021, Multiwavelength observations of a metric type-II event. *Astron. Astrophys.* **654**, A112. DOI. ADS.

Bain, H.M., Krucker, S., Glesener, L., Lin, R.P.: 2012, Radio imaging of shock-accelerated electrons associated with an erupting plasmoid on 2010 November 3. *Astrophys. J.* **750**, 44. DOI. ADS.

Balasubramaniam, K.S., Pevtsov, A.A., Neidig, D.F.: 2007, Are Moreton waves coronal phenomena? *Astrophys. J.* **658**, 1372. DOI. ADS.

Biesecker, D.A., Myers, D.C., Thompson, B.J., Hammer, D.M., Vourlidas, A.: 2002, Solar phenomena associated with "EIT waves". *Astrophys. J.* **569**, 1009. DOI. ADS.

Bogdanov, S.Y., Dreiden, G.V., Frank, A.G., Kirei, N.P., Khodzhaev, A.Z., Komissarova, I.I., Markov, V.S., Ostrovskaya, G.V., Ostrovsky, Y.I., Philippov, V.N., Savchenko, M.M., Shedova, E.N.: 1984, Plasma dynamics inside the current sheet. *Physica Scripta* **30**, 282. DOI. ADS.

Bougeret, J.L., Goetz, K., Kaiser, M.L., Bale, S.D., Kellogg, P.J., Maksimovic, M., Monge, N., Monson, S.J., Astier, P.L., Davy, S., *et al.*: 2008, S/WAVES: The Radio and Plasma Wave Investigation on the STEREO mission. *Space Sci. Rev.* **136**, 487. DOI. ADS.

Brueckner, G.E., Howard, R.A., Koomen, M.J., Korendyke, C.M., Michels, D.J., Moses, J.D., Socker, D.G., Dere, K.P., Lamy, P.L., Llebaria, A., *et al.*: 1995, The Large Angle Spectroscopic Coronagraph (LASCO). *Solar Phys.* **162**, 357. DOI. ADS.

Cane, H.V.: 1984, The relationship between coronal transients, Type II bursts and interplanetary shocks. *Astron. Astrophys.* **140**, 205. ADS.

Cane, H.V., Erickson, W.C.: 2005, Solar type II radio bursts and IP type II events. *Astrophys. J.* **623**, 1180. DOI. ADS.

Chen, P.F.: 2011, Coronal mass ejections: Models and their observational basis. *Liv. Rev. Solar Phys.* **8**, 1. DOI. ADS.

Chen, P.F., Wu, Y.: 2011, First evidence of coexisting EIT wave and coronal Moreton wave from SDO/AIA observations. *Astrophys. J. Lett.* **732**, L20. DOI. ADS.

Chen, P.F., Fang, C., Shibata, K.: 2005, A full view of EIT waves. *Astrophys. J.* **622**, 1202. DOI. ADS.

Chen, P.F., Wu, S.T., Shibata, K., Fang, C.: 2002, Evidence of EIT and Moreton waves in numerical simulations. *Astrophys. J. Lett.* **572**, L99. DOI. ADS.

Chen, Y., Du, G., Feng, L., Feng, S., Kong, X., Guo, F., Wang, B., Li, G.: 2014, A solar Type II radio burst from coronal mass ejection–coronal ray interaction: Simultaneous radio and extreme ultraviolet imaging. *Astrophys. J.* **787**, 59. DOI. ADS.

Cliver, E.W.: 2016, Flare vs. shock acceleration of high-energy protons in solar energetic particle events. *Astrophys. J.* **832**, 128. DOI. ADS.

Cliver, E.W., Nitta, N.V., Thompson, B.J., Zhang, J.: 2004, Coronal shocks of November 1997 revisited: The CME Type II timing problem. *Solar Phys.* **225**, 105. DOI. ADS.

Delaboudinière, J.-P., Artzner, G.E., Brunaud, J., Gabriel, A.H., Hochedez, J.F., Millier, F., Song, X.Y., Au, B., Dere, K.P., Howard, R.A., *et al.*: 1995, EIT: Extreme-Ultraviolet Imaging Telescope for the SOHO mission. *Solar Phys.* **162**, 291. DOI. ADS.

Dierckxsens, M., Tziotziou, K., Dalla, S., Patsou, I., Marsh, M.S., Crosby, N.B., Malandraki, O., Tsiropoula, G.: 2015, Relationship between solar energetic particles and properties of flares and CMEs: Statistical analysis of Solar Cycle 23 events. *Solar Phys.* **290**, 841. DOI. ADS.

Domingo, V., Fleck, B., Poland, A.I.: 1995, The SOHO mission: An overview. *Solar Phys.* **162**, 1. DOI. ADS.

Echer, E.: 2019, Solar wind and interplanetary shock parameters near Saturn's orbit (∼10 AU). *Planet. Space Sci.* **165**, 210. DOI. ADS.

Echer, E., Gonzalez, W.D., Tsurutani, B.T., Gonzalez, A.L.C.: 2008, Interplanetary conditions causing intense geomagnetic storms (Dst <= −100 nT) during solar cycle 23 (1996-2006). *J. Geophys. Res. (Space Phys.)* **113**, A05221. DOI. ADS.

Eselevich, V.G., Eselevich, M.V., Zimovets, I.V.: 2013, Blast-wave and piston shocks connected with the formation and propagation of a coronal mass ejection. *Astron. Rep.* **57**, 142. DOI. ADS.

Eselevich, V.G., Eselevich, M.V., Zimovets, I.V.: 2019, Observations of a flare-generated blast wave in a pseudo coronal mass ejection event. *Solar Phys.* **294**, 73. DOI. ADS.

Eselevich, V.G., Eselevich, M.V., Sadykov, V.M., Zimovets, I.V.: 2015, Evidence of a blast shock wave formation in a "CME-streamer" interaction. *Adv. Space Res.* **56**, 2793. DOI. ADS.

Fainshtein, V.G., Egorov, Y.I.: 2019, Onset of a CME-related shock within the Large-Angle Spectrometric Coronagraph (LASCO) field of view. *Solar Phys.* **294**, 126. DOI. ADS.

Feng, S.W., Chen, Y., Kong, X.L., Li, G., Song, H.Q., Feng, X.S., Liu, Y.: 2012, Radio signatures of coronal-mass-ejection-streamer interaction and source diagnostics of type II radio burst. *Astrophys. J.* **753**, 21. DOI. ADS.

Feng, S.W., Chen, Y., Kong, X.L., Li, G., Song, H.Q., Feng, X.S., Guo, F.: 2013, Diagnostics on the source properties of a Type II radio burst with spectral bumps. *Astrophys. J.* **767**, 29. DOI. ADS.

Gallagher, P.T., Long, D.M.: 2011, Large-scale bright fronts in the solar corona: A review of "EIT waves". *Space Sci. Rev.* **158**, 365. DOI. ADS.

Gopalswamy, N., Thompson, W.T., Davila, J.M., Kaiser, M.L., Yashiro, S., Mäkelä, P., Michalek, G., Bougeret, J.-L., Howard, R.A.: 2009, Relation between type II bursts and CMEs inferred from STEREO observations. *Solar Phys.* **259**, 227. DOI. ADS.

Gopalswamy, N., Xie, H., Yashiro, S., Akiyama, S., Mäkelä, P., Usoskin, I.G.: 2012, Properties of ground level enhancement events and the associated solar eruptions during Solar Cycle 23. *Space Sci. Rev.* **171**, 23. DOI. ADS.

Gopalswamy, N., Xie, H., Mäkelä, P., Yashiro, S., Akiyama, S., Uddin, W., Srivastava, A.K., Joshi, N.C., Chandra, R., Manoharan, P.K., Mahalakshmi, K., Dwivedi, V.C., Jain, R., Awasthi, A.K., Nitta, N.V., Aschwanden, M.J., Choudhary, D.P.: 2013, Height of shock formation in the solar corona inferred from observations of type II radio bursts and coronal mass ejections. *Advances in Space Research* **51**, 1981. DOI. ADS.

Gopalswamy, N., Xie, H., Akiyama, S., Mäkelä, P.A., Yashiro, S.: 2014, Major solar eruptions and high-energy particle events during solar cycle 24. *Earth, Planets and Space* **66**, 104. DOI. ADS.

Grechnev, V.V.: 2003, A method to analyze imaging radio data on solar flares. *Solar Phys.* **213**, 103. DOI. ADS.

Grechnev, V.V., Kuzmenko, I.V.: 2020, A geoeffective CME caused by the eruption of a quiescent prominence on 29 September 2013. *Solar Phys.* **295**, 55. DOI. ADS.

Grechnev, V.V., Uralov, A.M., Zandanov, V.G., Baranov, N.Y., Shibasaki, K.: 2006a, Observations of prominence eruptions with two radioheliographs, SSRT, and NoRH. *Publ. Astron. Soc. Japan* **58**, 69. DOI. ADS.

Grechnev, V.V., Uralov, A.M., Zandanov, V.G., Rudenko, G.V., Borovik, V.N., Grigorieva, I.Y., Slemzin, V.A., Bogachev, S.A., Kuzin, S.V., Zhitnik, I., Pertsov, A.A., Shibasaki, K., Livshits, M.A.: 2006b, Plasma parameters in a post-eruptive arcade observed with CORONAS-F/SPIRIT, Yohkoh/SXT, SOHO/EIT, and in microwaves. *Publ. Astron. Soc. Japan* **58**, 55. DOI. ADS.

Grechnev, V.V., Uralov, A.M., Slemzin, V.A., Chertok, I.M., Kuzmenko, I.V., Shibasaki, K.: 2008, Absorption phenomena and a probable blast wave in the 13 July 2004 eruptive event. *Solar Phys.* **253**, 263. DOI. ADS.

Grechnev, V.V., Uralov, A.M., Chertok, I.M., Kuzmenko, I.V., Afanasyev, A.N., Meshalkina, N.S., Kalashnikov, S.S., Kubo, Y.: 2011a, Coronal shock waves, EUV waves, and their relation to CMEs. I. Reconciliation of "EIT waves", type II radio bursts, and leading edges of CMEs. *Solar Phys.* **273**, 433. DOI. ADS.

Grechnev, V.V., Afanasyev, A.N., Uralov, A.M., Chertok, I.M., Eselevich, M.V., Eselevich, V.G., Rudenko, G.V., Kubo, Y.: 2011b, Coronal shock waves, EUV waves, and their relation to CMEs. III. Shock-associated CME/EUV wave in an event with a two-component EUV transient. *Solar Phys.* **273**, 461. DOI. ADS.

Grechnev, V.V., Kiselev, V.I., Uralov, A.M., Meshalkina, N.S., Kochanov, A.A.: 2013, An updated view of solar eruptive flares and the development of shocks and CMEs: History of the 2006 December 13 GLE-productive extreme event. *Publ. Astron. Soc. Japan* **65**, S9. DOI. ADS.

Grechnev, V.V., Uralov, A.M., Chertok, I.M., Slemzin, V.A., Filippov, B.P., Egorov, Y.I., Fainshtein, V.G., Afanasyev, A.N., Prestage, N.P., Temmer, M.: 2014, A challenging solar eruptive event of 18 November 2003 and the causes of the 20 November geomagnetic superstorm. II. CMEs, shock waves, and drifting radio bursts. *Solar Phys.* **289**, 1279. DOI. ADS.

Grechnev, V.V., Uralov, A.M., Kuzmenko, I.V., Kochanov, A.A., Chertok, I.M., Kalashnikov, S.S.: 2015, Responsibility of a filament eruption for the initiation of a flare, CME, and blast wave, and its possible transformation into a bow shock. *Solar Phys.* **290**, 129. DOI. ADS.

Grechnev, V.V., Uralov, A.M., Kochanov, A.A., Kuzmenko, I.V., Prosovetsky, D.V., Egorov, Y.I., Fainshtein, V.G., Kashapova, L.K.: 2016, A tiny eruptive filament as a flux-rope progenitor and driver of a large-scale CME and wave. *Solar Phys.* **291**, 1173. DOI. ADS.

Grechnev, V.V., Kiselev, V.I., Uralov, A.M., Klein, K.-L., Kochanov, A.A.: 2017, The 26 December 2001 solar eruptive event responsible for GLE63: III. CME, shock waves, and energetic particles. *Solar Phys.* **292**, 102. DOI. ADS.

Grechnev, V.V., Lesovoi, S.V., Kochanov, A.A., Uralov, A.M., Altyntsev, A.T., Gubin, A.V., Zhdanov, D.A., Ivanov, E.F., Smolkov, G.Y., Kashapova, L.K.: 2018a, Multi-instrument view on solar eruptive events observed with the Siberian Radioheliograph: From detection of small jets up to development of a shock wave and CME. *J. Atmos. Solar-Terr. Phys.* **174**, 46. DOI. ADS.

Grechnev, V.V., Kiselev, V.I., Kashapova, L.K., Kochanov, A.A., Zimovets, I.V., Uralov, A.M., Nizamov, B.A., Grigorieva, I.Y., Golovin, D.V., Litvak, M.L., Mitrofanov, I.G., Sanin, A.B.: 2018b, Radio, hard X-ray, and gamma-ray emissions associated with a far-side solar event. *Solar Phys.* **293**, 133. DOI. ADS.

Grechnev, V.V., Kochanov, A.A., Uralov, A.M., Slemzin, V.A., Rodkin, D.G., Goryaev, F.F., Kiselev, V.I., Myshyakov, I.I.: 2019, Development of a fast CME and properties of a related interplanetary transient. *Solar Phys.* **294**, 139. DOI. ADS.

Grechnev, V.V., Kiselev, V.I., Uralov, A.M., Myshyakov, I.I.: 2022, Reconciliation of Observational Challenges to the Impulsive-Piston Shock-Excitation Scenario. II. Shock Waves Produced in CME-less Events with a Null-Point Topology. *Solar Phys.*, *submitted*.

Green, L.M., Török, T., Vršnak, B., Manchester, W., Veronig, A.: 2018, The origin, early evolution and predictability of solar eruptions. *Space Sci. Rev.* **214**, 46. DOI. ADS.

Hirayama, T.: 1974, Theoretical model of flares and prominences. I: Evaporating flare model. *Solar Phys.* **34**, 323. DOI. ADS.

Howard, R.A., Moses, J.D., Vourlidas, A., Newmark, J.S., Socker, D.G., Plunkett, S.P., Korendyke, C.M., Cook, J.W., Hurley, A., Davila, J.M., *et al.*: 2008, Sun Earth Connection Coronal and Heliospheric Investigation (SECCHI). *Space Sci. Rev.* **136**, 67. DOI. ADS.

Hudson, H.S., Khan, J.I., Lemen, J.R., Nitta, N.V., Uchida, Y.: 2003, Soft X-ray observation of a large-scale coronal wave and its exciter. *Solar Phys.* **212**, 121. DOI. ADS.

Inhester, B., Birn, J., Hesse, M.: 1992, The evolution of line tied coronal arcades including a converging footpoint motion. *Solar Phys.* **138**, 257. DOI. ADS.

Kahler, S.W.: 2001, The correlation between solar energetic particle peak intensities and speeds of coronal mass ejections: Effects of ambient particle intensities and energy spectra. *J. Geophys. Res.* **106**, 20947. DOI. ADS.

Kaiser, M.L., Kucera, T.A., Davila, J.M., St. Cyr, O.C., Guhathakurta, M., Christian, E.: 2008, The STEREO mission: An introduction. *Space Sci. Rev.* **136**, 5. DOI. ADS.

Kalaivani, P.P., Prakash, O., Shanmugaraju, A., Feng, L., Lu, L., Gan, W., Michalek, G.: 2021, Analysis of type II and type III radio bursts associated with SEPs from non-interacting/interacting radio-loud CMEs. *Astrophysics* **64**, 327. DOI. ADS.

Klein, K.-L., Trottet, G.: 2001, The origin of solar energetic particle events: coronal acceleration versus shock wave acceleration. *Space Sci. Rev.* **95**, 215. ADS.

Knock, S.A., Cairns, I.H.: 2005, Type II radio emission predictions: Sources of coronal and interplanetary spectral structure. *J. Geophys. Res.* **110**, A01101. DOI. ADS.

Kumar, P., Innes, D.E.: 2013, Multiwavelength observations of an eruptive flare: Evidence for blast waves and break-out. *Solar Phys.* **288**, 255. DOI. ADS.

Kumar, P., Innes, D.E.: 2015, Partial reflection and trapping of a fast-mode wave in solar coronal arcade loops. *Astrophys. J. Lett.* **803**, L23. DOI. ADS.

Kumar, P., Innes, D.E., Cho, K.-S.: 2016, Flare-generated shock wave propagation through solar coronal arcade loops and an associated Type II radio burst. *Astrophys. J.* **828**, 28. DOI. ADS.

Landau, L.D., Lifshitz, E.M.: 1987, *Fluid Mechanics*, Pergamon Press, Oxford.

Lemen, J.R., Title, A.M., Akin, D.J., Boerner, P.F., Chou, C., Drake, J.F., Duncan, D.W., Edwards, C.G., Friedlaender, F.M., Heyman, G.F., *et al.*: 2012, The Atmospheric Imaging Assembly (AIA) on the Solar Dynamics Observatory (SDO). *Solar Phys.* **275**, 17. DOI. ADS.

Lependin, L.F.: 1978, *Acoustics*, Graduate School, Moscow.

Liu, W., Ofman, L.: 2014, Advances in observing various coronal EUV waves in the SDO era and their seismological applications (invited review). *Solar Phys.* **289**, 3233. DOI. ADS.

Liu, Y., Luhmann, J.G., Müller-Mellin, R., Schroeder, P.C., Wang, L., Lin, R.P., Bale, S.D., Li, Y., Acuña, M.H., Sauvaud, J.-A.: 2008, A comprehensive view of the 2006 December 13 CME: From the Sun to interplanetary space. *Astrophys. J.* **689**, 563. DOI. ADS.

Long, D.M., Murphy, P., Graham, G., Carley, E.P., Pérez-Suárez, D.: 2017, A statistical analysis of the solar phenomena associated with global EUV waves. *Solar Phys.* **292**, 185. DOI. ADS.

Longcope, D.W., Beveridge, C.: 2007, A quantitative, topological model of reconnection and flux rope formation in a two-ribbon flare. *Astrophys. J.* **669**, 621. DOI. ADS.

Low, B.C.: 1982, Self-similar magnetohydrodynamics. I - The gamma = 4/3 polytrope and the coronal transient. *Astrophys. J.* **254**, 796. DOI. ADS.

Luhmann, J.G., Curtis, D.W., Schroeder, P., McCauley, J., Lin, R.P., Larson, D.E., Bale, S.D., Sauvaud, J.-A., Aoustin, C., Mewaldt, R.A., *et al.*: 2008, STEREO IMPACT investigation goals, measurements, and data products overview. *Space Sci. Rev.* **136**, 117. DOI. ADS.

Lulić, S., Vršnak, B., Žic, T., Kienreich, I.W., Muhr, N., Temmer, M., Veronig, A.M.: 2013, Formation of coronal shock waves. *Solar Phys.* **286**, 509. DOI. ADS.

Magdalenić, J., Vršnak, B., Pohjolainen, S., Temmer, M., Aurass, H., Lehtinen, N.J.: 2008, A flare-generated shock during a coronal mass ejection on 24 December 1996. *Solar Phys.* **253**, 305. DOI. ADS.

Magdalenić, J., Marqué, C., Zhukov, A.N., Vršnak, B., Žic, T.: 2010, Origin of coronal shock waves associated with slow coronal mass ejections. *Astrophys. J.* **718**, 266. DOI. ADS.

Magdalenić, J., Marqué, C., Zhukov, A.N., Vršnak, B., Veronig, A.: 2012, Flare-generated Type II burst without associated coronal mass ejection. *Astrophys. J.* **746**, 152. DOI. ADS.

Mancuso, S., Raymond, J.C.: 2004, Coronal transients and metric Type II radio bursts. I. Effects of geometry. *Astron. Astrophys.* **413**, 363. DOI. ADS.

Mann, G., Klassen, A., Aurass, H., Classen, H.-T.: 2003, Formation and development of shock waves in the solar corona and the near-Sun interplanetary space. *Astron. Astrophys.* **400**, 329. DOI. ADS.

Maričić, D., Vršnak, B., Stanger, A.L., Veronig, A.M., Temmer, M., Roša, D.: 2007, Acceleration phase of coronal mass ejections: II. Synchronization of the energy release in the associated flare. *Solar Phys.* **241**, 99. DOI. ADS.

Miklenic, C.H., Veronig, A.M., Vršnak, B.: 2009, Temporal comparison of nonthermal flare emission and magnetic-flux change rates. *Astron. Astrophys.* **499**, 893. DOI. ADS.

Moreton, G.E.: 1960, Hα observations of flare-initiated disturbances with velocities ~1000 km/sec. *Astronom. J.* **65**, 494. DOI. ADS.

Moses, D., Clette, F., Delaboudinière, J.-P., Artzner, G.E., Bougnet, M., Brunaud, J., Carabetian, C., Gabriel, A.H., Hochedez, J.F., Millier, F., *et al.*: 1997, EIT observations of the extreme ultraviolet Sun. *Solar Phys.* **175**, 571. DOI. ADS.

Neupert, W.M.: 1968, Comparison of solar X-ray line emission with microwave emission during flares. *Astrophys. J. Lett.* **153**, L59. DOI. ADS.

Nindos, A., Alissandrakis, C.E., Gelfreikh, G.B., Bogod, V.M., Gontikakis, C.: 2002, Spatially resolved microwave oscillations above a sunspot. *Astron. Astrophys.* **386**, 658. DOI. ADS.

Nindos, A., Alissandrakis, C.E., Hillaris, A., Preka-Papadema, P.: 2011, On the relationship of shock waves to flares and coronal mass ejections. *Astron. Astrophys.* **531**, A31. DOI. ADS.

Nitta, N.V., Schrijver, C.J., Title, A.M., Liu, W.: 2013, Large-scale coronal propagating fronts in solar eruptions as observed by the Atmospheric Imaging Assembly on board the Solar Dynamics Observatory—an ensemble study. *Astrophys. J.* **776**, 58. DOI. ADS.

Patsourakos, S., Vourlidas, A.: 2012, On the nature and genesis of EUV waves: A synthesis of observations from SOHO, STEREO, SDO, and Hinode (invited review). *Solar Phys.* **281**, 187. DOI. ADS.

Pesnell, W.D., Thompson, B.J., Chamberlin, P.C.: 2012, The Solar Dynamics Observatory (SDO). *Solar Phys.* **275**, 3. DOI. ADS.

Qiu, J., Hu, Q., Howard, T.A., Yurchyshyn, V.B.: 2007, On the magnetic flux budget in low-corona magnetic reconnection and interplanetary coronal mass ejections. *Astrophys. J.* **659**, 758. DOI. ADS.

Reames, D.V.: 2009, Solar release times of energetic particles in ground-level events. *Astrophys. J.* **693**, 812. DOI. ADS.

Reames, D.V.: 2013, The two sources of solar energetic particles. *Space Sci. Rev.* **175**, 53. DOI. ADS.

Reiner, M.J., Vourlidas, A., Cyr, O.C.S., Burkepile, J.T., Howard, R.A., Kaiser, M.L., Prestage, N.P., Bougeret, J.-L.: 2003, Constraints on coronal mass ejection dynamics from simultaneous radio and white-light observations. *Astrophys. J.* **590**, 533. DOI. ADS.

Rouillard, A.P., Plotnikov, I., Pinto, R.F., Tirole, M., Lavarra, M., Zucca, P., Vainio, R., Tylka, A.J., Vourlidas, A., De Rosa, M.L., *et al.*: 2016, Deriving the properties of coronal pressure fronts in 3D: Application to the 2012 May 17 ground level enhancement. *Astrophys. J.* **833**, 45. DOI. ADS.

Saito, K., Makita, M., Nishi, K., Hata, S.: 1970, A non-spherical axisymmetric model of the solar K corona of the minimum type. *Ann. Tokyo Astron. Observ.* **12**, 53. ADS.

Shen, C., Liao, C., Wang, Y., Ye, P., Wang, S.: 2013, Source region of the decameter-hectometric type II radio burst: Shock-streamer interaction region. *Solar Phys.* **282**, 543. DOI. ADS.

Su, W., Cheng, X., Ding, M.D., Chen, P.F., Sun, J.Q.: 2015, A Type II radio burst without a coronal mass ejection. *Astrophys. J.* **804**, 88. DOI. ADS.

Temmer, M., Veronig, A.M., Vršnak, B., Rybák, J., Gömöry, P., Stoiser, S., Maričić, D.: 2008, Acceleration in fast halo CMEs and synchronized flare HXR bursts. *Astrophys. J. Lett.* **673**, L95. DOI. ADS.

Temmer, M., Veronig, A.M., Kontar, E.P., Krucker, S., Vršnak, B.: 2010, Combined STEREO/RHESSI study of coronal mass ejection acceleration and particle acceleration in solar flares. *Astrophys. J.* **712**, 1410. DOI. ADS.

Thalmann, J.K., Su, Y., Temmer, M., Veronig, A.M.: 2015, The confined X-class flares of solar active region 2192. *Astrophys. J. Lett.* **801**, L23. DOI. ADS.

Thompson, B.J., Plunkett, S.P., Gurman, J.B., Newmark, J.S., St. Cyr, O.C., Michels, D.J.: 1998, SOHO/EIT observations of an Earth-directed coronal mass ejection on May 12, 1997. *Geophys. Res. Lett.* **25**, 2465. DOI. ADS.

Thompson, B.J., Gurman, J.B., Neupert, W.M., Newmark, J.S., Delaboudinière, J.-P., Cyr, O.C.S., Stezelberger, S., Dere, K.P., Howard, R.A., Michels, D.J.: 1999, SOHO/EIT observations of the 1997 April 7 coronal transient: Possible evidence of coronal Moreton waves. *Astrophys. J. Lett.* **517**, L151. DOI. ADS.

Trottet, G., Samwel, S., Klein, K.-L., Dudok de Wit, T., Miteva, R.: 2015, Statistical evidence for contributions of flares and coronal mass ejections to major solar energetic particle events. *Solar Phys.* **290**, 819. DOI. ADS.

Uchida, Y.: 1968, Propagation of hydromagnetic disturbances in the solar corona and Moreton's wave phenomenon. *Solar Phys.* **4**, 30. DOI. ADS.

Uchida, Y.: 1974, Behaviour of the flare-produced coronal MHD wavefront and the occurrence of type II radio bursts. *Solar Phys.* **39**, 431. DOI. ADS.

Uralov, A.M., Grechnev, V.V., Hudson, H.S.: 2005, Initial localization and kinematic characteristics of the structural components of a coronal mass ejection. *J. Geophys. Res. (Space Phys.)* **110**, A05104. DOI. ADS.

Uralov, A.M., Grechnev, V.V., Ivanukin, L.A.: 2019, Self-similar piston-shock and CME. *Solar Phys.* **294**, 113. DOI. ADS.

Uralov, A.M., Lesovoi, S.V., Zandanov, V.G., Grechnev, V.V.: 2002, Dual-filament initiation of a coronal mass ejection: Observations and model. *Solar Phys.* **208**, 69. DOI. ADS.

Uralova, S.V., Uralov, A.M.: 1994, WKB approach to the problem of magnetohydrodynamic shock propagation through the heliospheric current sheet. *Solar Phys.* **152**, 457. DOI. ADS.

Veselovsky, I.S., Panasyuk, M.I., Avdyushin, S.I., Bazilevskaya, G.A., Belov, A.V., Bogachev, S.A., Bogod, V.M., Bogomolov, A.V., Bothmer, V., Boyarchuk, K.A., *et al.*: 2004, Solar and Heliospheric Phenomena in October-November 2003: Causes and Effects. *Cosmic Research* **42**, 435. DOI. ADS.

Vourlidas, A., Wu, S.T., Wang, A.H., Subramanian, P., Howard, R.A.: 2003, Direct detection of a coronal mass ejection-associated shock in Large Angle and Spectrometric Coronagraph experiment white-light images. *Astrophys. J.* **598**, 1392. DOI. ADS.

Vršnak, B., Cliver, E.W.: 2008, Origin of coronal shock waves. Invited review. *Solar Phys.* **253**, 215. DOI. ADS.

Vršnak, B.: 2016, Solar eruptions: The CME-flare relationship. *Astron. Nachr.* **337**, 1002. DOI. ADS.

Vršnak, B., Warmuth, A., Brajša, R., Hanslmeier, A.: 2002, Flare waves observed in Helium I 10 830 Å. A link between Hα Moreton and EIT waves. *Astron. Astrophys.* **394**, 299. DOI. ADS.

Žic, T., Vršnak, B., Temmer, M., Jacobs, C.: 2008, Cylindrical and spherical pistons as drivers of MHD shocks. *Solar Phys.* **253**, 237. DOI. ADS.

Warmuth, A.: 2007, In: Klein, K.-L., MacKinnon, A.L. (eds.) *Large-scale waves and shocks in the solar corona* **725**, 107. ADS.
Warmuth, A.: 2010, Large-scale waves in the solar corona: The continuing debate. *Adv. Space Res.* **45**, 527. DOI. ADS.
Warmuth, A.: 2015, Large-scale globally propagating coronal waves. *Liv. Rev. Solar Phys.* **12**, 3. DOI. ADS.
Warmuth, A., Mann, G.: 2011, Kinematical evidence for physically different classes of large-scale coronal EUV waves. *Astron. Astrophys.* **532**, A151. DOI. ADS.
Warmuth, A., Mann, G., Aurass, H.: 2005, First soft X-ray observations of global coronal waves with the GOES Solar X-ray Imager. *Astrophys. J. Lett.* **626**, L121. DOI. ADS.
Warmuth, A., Vršnak, B., Aurass, H., Hanslmeier, A.: 2001, Evolution of two EIT/Hα Moreton waves. *Astrophys. J. Lett.* **560**, L105. DOI. ADS.
Warmuth, A., Vršnak, B., Magdalenić, J., Hanslmeier, A., Otruba, W.: 2004a, A multiwavelength study of solar flare waves. I. Observations and basic properties. *Astron. Astrophys.* **418**, 1101. DOI. ADS.
Warmuth, A., Vršnak, B., Magdalenić, J., Hanslmeier, A., Otruba, W.: 2004b, A multiwavelength study of solar flare waves. II. Perturbation characteristics and physical interpretation. *Astron. Astrophys.* **418**, 1117. DOI. ADS.
White, S.M., Thompson, B.J.: 2005, High-cadence radio observations of an EIT wave. *Astrophys. J. Lett.* **620**, L63. DOI. ADS.
Yashiro, S., Gopalswamy, N., Michalek, G., St. Cyr, O.C., Plunkett, S.P., Rich, N.B., Howard, R.A.: 2004, A catalog of white light coronal mass ejections observed by the SOHO spacecraft. *J. Geophys. Res. (Space Phys.)* **109**, A07105. DOI. ADS.
Zhang, J., Dere, K.P., Howard, R.A., Kundu, M.R., White, S.M.: 2001, On the temporal relationship between coronal mass ejections and flares. *Astrophys. J.* **559**, 452. DOI. ADS.
Zhukov, A.N., Auchère, F.: 2004, On the nature of EIT waves, EUV dimmings and their link to CMEs. *Astron. Astrophys.* **427**, 705. DOI. ADS.
Zhukov, A.N., Rodriguez, L., de Patoul, J.: 2009, STEREO/SECCHI observations on 8 December 2007: Evidence against the wave hypothesis of the EIT wave origin. *Solar Phys.* **259**, 73. DOI. ADS.
Zimovets, I., Vilmer, N., Chian, A.C.-L., Sharykin, I., Struminsky, A.: 2012, Spatially resolved observations of a split-band coronal Type II radio burst. *Astron. Astrophys.* **547**, A6. DOI. ADS.